frontiers | Frontiers in Immunology

TYPE Original Research
PUBLISHED 29 April 2024
DOI 10.3389/fimmu.2024.1372904

OPEN ACCESS

EDITED BY
Rita Marino,
Anton Dohrn Zoological Station Naples, Italy

REVIEWED BY
Guan-Jun Yang,
Ningbo University, China
Jeswin Joseph,
Cochin University of Science and Technology, India
Ojas Natarajan,
University of South Florida, United States

*CORRESPONDENCE
L Courtney Smith
csmith@gwu.edu

RECEIVED 18 January 2024
ACCEPTED 29 March 2024
PUBLISHED 29 April 2024

CITATION
Crow RS, Shaw CG, Grayfer L and Smith LC (2024) Recombinant SpTransformer proteins are functionally diverse for binding and phagocytosis by three subtypes of sea urchin phagocytes.
Front. Immunol. 15:1372904.
doi: 10.3389/fimmu.2024.1372904

Recombinant SpTransformer proteins are functionally diverse for binding and phagocytosis by three subtypes of sea urchin phagocytes

Ryley S. Crow, Chloe G. Shaw, Leon Grayfer and L Courtney Smith*

Department of Biological Sciences, George Washington University, Washington, DC, United States

Introduction: The California purple sea urchin, *Strongylocentrotus purpuratus*, relies solely on an innate immune system to combat the many pathogens in the marine environment. One aspect of their molecular defenses is the *SpTransformer* (*SpTrf*) gene family that is upregulated in response to immune challenge. The gene sequences are highly variable both within and among animals and likely encode thousands of SpTrf isoforms within the sea urchin population. The native SpTrf proteins bind foreign targets and augment phagocytosis of a marine *Vibrio*. A recombinant (r)SpTrf-E1-Ec protein produced by *E. coli* also binds *Vibrio* but does not augment phagocytosis.

Methods: To address the question of whether other rSpTrf isoforms function as opsonins and augment phagocytosis, six rSpTrf proteins were expressed in insect cells.

Results: The rSpTrf proteins are larger than expected, are glycosylated, and one dimerized irreversibly. Each rSpTrf protein cross-linked to inert magnetic beads (rSpTrf::beads) results in different levels of surface binding and phagocytosis by phagocytes. Initial analysis shows that significantly more rSpTrf::beads associate with cells compared to control BSA::beads. Binding specificity was verified by pre-incubating the rSpTrf::beads with antibodies, which reduces the association with phagocytes. The different rSpTrf::beads show significant differences for cell surface binding and phagocytosis by phagocytes. Furthermore, there are differences among the three distinct types of phagocytes that show specific vs. constitutive binding and phagocytosis.

Conclusion: These findings illustrate the complexity and effectiveness of the sea urchin innate immune system driven by the natSpTrf proteins and the phagocyte cell populations that act to neutralize a wide range of foreign pathogens.

KEYWORDS

***Strongylocentrotus purpuratus*, polygonal phagocyte, discoidal phagocyte, small phagocyte, inert beads**

1 Introduction

Innate immune systems function with a variety of pathogen recognition receptors (PRRs) that are located on the cell surface, the endomembrane system, in the cytoplasm, or secreted into the extracellular fluid. Well studied PRRs include Toll-like receptors (TLRs) (1–3), NOD-like receptors (NLRs) (4, 5), RIG-I-like receptors (RLRs) (6, 7), C-type lectin receptors (CLRs) (8), as well as resistance (R) proteins in plants (9, 10). PRR recognition of immunological insult is the core of all metazoan defenses and have key functions in invertebrate species, which lack immune receptor genes that are built by somatic recombination or copy choice that confer adaptive immunity in vertebrates (11–13). In response to PRR signaling, organisms secrete a wide variety of effector proteins that include expanded gene families encoding anti-microbial peptides and proteins (AMPs) (14–17). Invertebrates such as sea urchins have a sophisticated innate immune system with expanded gene families encoding TLRs, NLRs [(18, 19); reviewed in (20, 21)], small C-type lectins (19), and a variety of AMPs that function in a wide range of organisms (16, 22, 23). The purple sea urchin from the Pacific coast of North America, *Strongylocentrotus purpuratus*, also has the *SpTransformer* (*SpTrf*) gene family [reviewed in (24)] that encodes unique immune effector proteins. The *Trf* genes are found exclusively in euechinoids and have been reported in purple sea urchins in Australia, *Heliocidaris erythrogramma*, *HeTrf* (25) and in the Mediterranean, *Paracentrotus lividus*, *PlTrf* (26). The *Trf* gene sequences are similar among the sea urchin species, but fall into phylogenetically separate clades (25, 26).

The *SpTrf* gene family was initially identified based on significantly elevated expression in response to challenge with marine bacteria (27) and to a variety of pathogen associated molecular patterns (PAMPs) (28–30). This expression pattern is consistent with immune response functions of the encoded proteins. Furthermore, full length sequences of the *SpTrf* cDNAs and genes show a significant level of sequence diversity, in part based on single nucleotide polymorphisms that translate to amino acid diversity. Optimized alignments require the insertion of large artificial gaps that define blocks of slightly variable sequences termed 'elements' (Figure 1) (30, 31, 33, 34). Elements of different sequence and length are present in the HeTrf and PlTrf proteins, although some of the repeats in the coding region are similar to those in SpTrf (25, 26). *In silico* analyses (DisMeta server (https://montelionelab.chem.rpi.edu/dismeta/)) predicts that the Trf proteins are all entirely disordered, which is supported by results from circular dichroism of one recombinant version (r)SpTrf-E1 expressed in *E. coli* (rSpTrf-E1-Ec) (35, 36) and by AlphaFold (DeepMind.com) for several Trf proteins.

The Trf proteins in *S. purpuratus* and *H. erythrogramma* are expressed by the phagocyte class of coelomocytes in response to immune challenge, with elevated expression in the polygonal, medium, and small phagocytes and much lower expression in discoidal phagocytes (25, 29, 37–39); [reviewed in (24)]. All Trf proteins have the same general structure of a leader followed by a glycine-rich region, a central multimerization region, a histidine-rich region, and a C terminal region (Figure 1; Supplementary Figure S1) and although all Trf proteins from all species multimerize irreversibly, their multimerization motifs are dissimilar (25, 26, 30, 35, 37, 40). As indicated by the leader, the SpTrf proteins are secreted into the coelomic fluid (CF), which was verified experimentally (38, 41).

Many versions of native (nat)SpTrf proteins with sufficient numbers of histidines in their histidine-rich region (Supplementary Figures S1, S2) can be isolated collectively by nickel affinity (42). They bind to Gram positive and negative bacteria and to yeast, and augment phagocytosis when bound to *Vibrio diazotrophicus* (38). However, nickel affinity does not allow differential isolation of individual natSpTrf proteins. Therefore, to understand the functions of individual SpTrf proteins, rather than all SpTrf proteins functioning together, rSpTrf-E1-Ec was investigated and found to have multiple binding targets. It binds LPS, flagellin, phosphatidic acid, β-1,3-glucan, *Vibrio diazotrophicus*, and *Saccharomyces cerevisiae*, however, it does not bind to peptidoglycan or *Bacillus* spp (35, 40). Upon the addition of LPS or phosphatidic acid, among other negatively charged molecules, rSpTrf-E1-Ec undergoes a structural transformation from disordered to mostly alpha helical (36, 40). Based on this unexpected characteristic, the proteins were re-named from the original of Sp185/333 to SpTransformer (SpTrf) with a concurrent renaming of the genes and messages. We have speculated that the sequence diversity among the natSpTrf proteins confers different multitasking functions that may overlap and provide maximal protection for sea urchins against pathogens (35), reviewed in

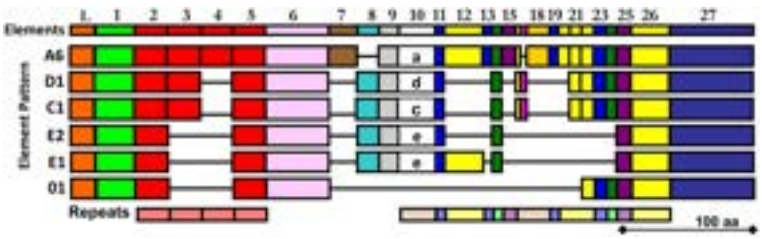

FIGURE 1
The alignment illustrates the mosaic element patterns in the rSpTrf proteins chosen for expression in insect cells. Elements are recognizable blocks of sequence that are slightly variable, and are defined by gaps in an alignment of all known SpTrf protein sequences deduced from cDNA and gene sequences (30, 31). Elements are depicted as colored rectangles. All possible elements are numbered at the top of the alignment. There are no SpTrf sequences that include all elements. Both tandem and interspersed repeats are shown below the alignment. This figure is modified from (32).

(24)). Many different versions of the SpTrf proteins are expressed in response to immune challenge (43, 44) and may function optimally when secreted together into the CF. Surprisingly, rSpTrf-E1-Ec binds to *Vibrio diazotrophicus* but does not enhance phagocytosis of the bacteria by sea urchin phagocytes (38). Consequently, we proposed that the natSpTrf proteins with an E1 element pattern may function with other versions of natSpTrf proteins to drive phagocytosis of foreign and invading cells in *S. purpuratus*.

Previous work has shown that *E. coli* fails to express SpTrf proteins, with the exception of rSpTrf-E1-Ec (35). Consequently, to address the hypothesis of functional diversity among the SpTrf proteins, six were expressed in recombinant form through a eukaryotic expression system using Sf9 insect cells, *Spodoptera frugiperda* (45). Proteins were chosen based on differences in their element patterns (Figure 1) and gene expression levels in sea urchins (30, 33). Each of the six rSpTrf proteins are larger than expected relative to amino acid sequences deduced from the cDNAs, and all are glycosylated with N-linked oligosaccharides. They are stable compared to the non-glycosylated rSpTrf-E1-Ec, although one dimerized over time without loss of function. When cross-linked to inert beads (rSpTrf::beads), a subset of the proteins, including the dimerized version, augments phagocytosis by a subset of sea urchin phagocytes. Phagocytosis of rSpTrf::beads is enhanced by the polygonal and small phagocytes, whereas the discoidal phagocytes show low levels of base-line, constitutive phagocytosis. Our findings indicate that the polygonal and small phagocytes recognize and bind distinct rSpTrf proteins. This infers that at least some of the natSpTrf proteins secreted into the CF act as opsonins in the sea urchin immune system and that the polygonal phagocytes are the major cellular responders to targets opsonized by the natSpTrf proteins. This highlights the crucial functions of the natSpTrf proteins in the detection and elimination of microbes and other foreign particles from the CF and internal tissues and organs.

2 Materials and methods

2.1 Expression and isolation of rSpTrf proteins

Recombinant protein expression in Sf9 cells and isolation by nickel affinity was based on the method of Hossainey et al. (46, 47). Coding sequences from cDNAs encoding six SpTrf proteins (Figure 1; Table 1) were used to produce expression constructs with the *pMIB/V5-His* expression vector (ThermoFisher) by Gibson assembly (Gibson Assembly Cloning Kit, New England Biolabs). Coding sequence in the *pMIB/V5-His* vector adds a V5 tag and six histidines to the C terminus of the recombinant proteins. cDNA inserts and *pMIB/V5-His* were amplified with Gibson primers (Supplementary Table S2). The leader sequences in the deduced SpTrf proteins were identified by Signal P (ver 5.0; https://services.healthtech.dtu.dk/service.php?SignalP-5.0) and omitted from the amplicons as in Lun et al. (35). The truncated version of SpTrf-E2 was generated with a primer that inserted an early stop codon to result in rSpTrf-E2.1 (Supplementary Figure S2, Supplementary Table S1). Gibson assemblies were transfected into *E. coli* (Top 10 chemically competent, Invitrogen), selected with ampicillin, and the expected insert sizes of transfectants were confirmed by PCR. The cDNA encoding SpTrf-E2 was also used in standard vector construction by amplifying the insert using primers with *Hind*III and *Xho*I sequences (Supplementary Table S2) followed by restriction digests and ligation into the multiple cloning site in

TABLE 1 rSpTrf protein sizes and predicted sites for post-translational modifications.

rSpTrf protein	Deduced size (kDa)[1]	Observed size range (kDa)[2]	Number of bands (WB)	Conserved sites for oligosaccharides[3]		PNGaseF treatment (kDa)[5]	cDNA Accession number	cDNA clone[6]	cDNA insert size (nt)
				N-linked[4]	O-linked				
01	29.85	43 – 50	2	4	17	43 to 38 50 to 44	EF065909	8-2441	826
E1	36.45	45 – 60	1	7	18	60 to 50	DQ183168	Sp0032	1119
E2-3	32.14	45 – 50	2	5	13	45 to 34 50 to 43	EF065832	2-2439	934
E2-4	32.14	45 – 80	2	5	13	80 to 70			
C1	42.35	55 – 70	1	7	15	70 to 60	EF066287	2-1514	1151
D1	41.72	45 – 60	1	7	20	55 to 45	EF066028	9-1542	1135
A6	54.63	65 – 75	1	7	18	75 to 70	EF065991	9-1525	1474

[1]Size prediction is based on the cDNA sequence that was amplified and used to generate the *pMIB/V5-HisA* expression construct. The deduced amino acid sequence was evaluated with the ExPASy MW calculator tool (https://web.expasy.org/compute_pi/).
[2]Protein size variation is based on multiple Western blot analyses over time.
[3]The number of sites predicted for N-linked and O-linked oligosaccharide addition is based on searches of the amino acid sequences with https://services.healthtech.dtu.dk/services/NetNGlyc-1.0 and https://services.healthtech.dtu.dk/services/NetOGlyc-4.0/, respectively.
[4]See also Supplementary File 1, Supplementary Table S1.
[5]Change in protein size from deglycosylation of N-linked oligosaccharides.
[6]cDNA sequences are reported in Terwilliger et al. (30, 33).

digested *pMIB/V5-His*. Selected constructs were sequenced across the ligation regions (GeneWiz/Azenta) to verify that the reading frame was maintained. Constructs with open reading frames for each of the rSpTrf proteins were transfected into Sf9 insect cells using cellfectin II (ThermoFisher) according to manufacturer's instructions. Insect cell cultures were grown in Sf 900 II serum-free medium (Invitrogen) with gentamycin (15 µg/ml, ThermoFisher), and transfected cells were selected with blasticidin (10 µg/ml; Invitrogen). Preliminary protein expression and secretion into the culture medium was confirmed by Western Blot (see below) using rabbit-anti-V5-HRP antibody (Invitrogen). The culture was scaled up to 500 ml, the cells were pelleted, the culture medium was loaded into snakeskin dialysis tubing (3.5 kDa MW cut-off, 35 mm diameter, ThermoFisher), concentrated against polyethylene glycol flakes (PEG, 8000 MW; ThermoFisher) at 4°C for up to 8 hr or to about 85-120 ml, followed by dialysis against phosphate buffer (150 mM $NaPO_4$ pH 8 or PBS pH 8) at 4°C for 16 to 48 hrs. The concentrated culture medium was spun at 600 x *g* to pellet aggregates and the supernatant was diluted with an equal volume of binding/wash buffer (500 mM NaCl, 50 mM $NaPO_4$, 20 - 40 mM imidazole, pH 8) and incubated with 1.5 ml of washed Ni-NTA agarose beads (Qiagen) for 1 hr at room temperature (rt) with gentle rocking or rotation. Beads were pelleted at 60 x *g*, loaded into a 5 ml column, and washed 3 to 7 times with 5-7 ml of binding/wash buffer. rSpTrf proteins were eluted 5 to 7 times with 1 ml of elution buffer (binding/wash buffer with 250 mM imidazole), which were combined and loaded into snakeskin dialysis tubing, concentrated to ~1 ml on dry PEG, and dialyzed against PBS or phosphate buffer (pH 7.4) for 24 to 48 hrs at 4°C. The concentrated proteins were aliquoted and stored at -80°C. HALT (1%; Life Technologies) protease inhibitor was added to some samples. rSpTrf protein concentration was evaluated by OD^{205} on a spectrophotometer (Nanodrop 2000c [ThermoFisher] or NanodropOne [Thermo Scientific]) according to (36). The Scopes method (48) was used because the proteins do not have sufficient numbers of tryptophans, tyrosines, or cysteines in their sequences to be detected at OD^{280}.

2.2 Western blots

rSpTrf proteins (1-2 µg) were separated by 8-12% SDS PAGE and transferred to PVDF membranes (Immobilon-P^{seq}, EMD Millipore) for 10 min in a Trans-blot Turbo transfer system (BioRad). Filters were rinsed in Tris NaCl (TN, 25 mM Tris pH 7.4, 0.5 M NaCl) and blocked in blotto (5% milk in TN with 0.1% Tween 20 (TNT)) with rocking for 1.5 hrs at rt or overnight at 4°C. rSpTrf proteins were detected with rabbit-anti-V5-HRP (1500X to 3000X dilution in blotto; ThermoFisher). natSpTrf proteins on Western blots were detected with three rabbit-anti-natSpTrf-66, -68, -71 (3000 dilution each in blotto) that recognized different regions of the SpTrf proteins (Supplementary Figure S2), followed by goat-anti-rabbit-Ig-HRP (3000X dilution in blotto, Abcam) with rocking for 1 hour at rt (37). Filters were washed twice in TNT and twice in TN and incubated in ECL (Super Signal West Pico PLUS, ThermoScientific) and evaluated for chemiluminescence in a ChemiDoc Touch Imaging System (BioRad).

2.3 Deglycosylation

Conserved sites for N-linked and O-linked oligosaccharides in the sequences of the rSpTrf proteins were predicted using the online tools, https://services.healthtech.dtu.dk/services/NetNGlyc-1.0 and https://services.healthtech.dtu.dk/services/NetOGlyc-4.0/. Each rSpTrf protein (1-2 µg) or cell free CF (cfCF, 10-15 µl) was incubated with PNGaseF (1 µl, 0.5 U), *O*-glycosidase (2 µl, $8X10^4$ U), or *O*-glycosidase plus neuraminidase (2 µl, 40 U) at 37°C for 30 min, 75°C for 10 min, and chilled to 4°C according to the manufacturer's protocol (New England Biolabs). Protein sizes were evaluated by Western blot as described above. Control proteins were incubated without the glycosidases.

2.4 Isolation of natSpTrf proteins by Ni affinity

CF was collected from 12 to 15 sea urchins in calcium and magnesium free sea water with EDTA and HEPES buffer [CMFSW-EH; 460 mM NaCl, 10.7 mM KCl, 7.04 mM Na_2SO_4, 2.38 mM $NaHCO_3$, 70 mM EDTA, 20 mM HEPES pH 7.4 (44, 49)] and the cells were pelleted. The supernatant, or cfCF, was aliquoted and stored at -80°C until used. cfCF (35 ml) was incubated with washed Ni-NTA beads (1.75 ml; Invitrogen) by rotation at rt for 1 hr. Beads were pelleted at 800 x *g*, loaded into a 5 ml polypropylene column (ThermoFisher) and washed 3 times with 7 ml binding/wash buffer. Bound proteins were eluted 7 times with 1 ml elution buffer (10 mM NaCl, 50 mM $NaPO_4$, 300 mM imidazole) for each elution. Elutions were combined, loaded into snakeskin dialysis tubing or a Slide-a-Lyzer mini dialysis unit (10,000 MWCO; ThermoFisher), and concentrated against polyethylene glycol 8000 (ThermoFisher) for 1-2 hrs at 4°C followed by dialysis against PBS (pH 7.4) over night at 4°C. Protein concentration was evaluated at OD^{205} according to Scopes (48). The natSpTrf proteins eluted from the Ni affinity column and unbound proteins were evaluated by Western blot with rabbit anti-SpTrf antibodies, and goat-anti-rabbit-Ig-HRP as described above. The natSpTrf proteins were aliquoted and stored at -80°C until used.

2.5 rSpTrf proteins cross-linked to magnetic beads

Magnefy magnetic beads (1 µm, Bangs Laboratories) with COOH groups on the surface were washed 3 times in MiliQ water (1 ml) according to the manufacturer to remove contaminants in the storage buffer (0.05% NaN_3 in either de-ionized water or 5 mM Tris, 150 mM NaCl, Bangs Laboratory) and to reduce bead aggregation. Washed beads were incubated with 1-ethyl-3-(3-dimethyl-aminopropyl) carbodiimide hydrochloride (EDAC; PolyLink Protein Coupling Kit; Polysciences) in 200 µL for 15 min on a rotator at rt, followed by two wash steps using 200 µL coupling buffer as recommended to reduce bead aggregation. Beads were resuspended into 200 µL coupling buffer with each of the rSpTrf proteins or BSA (0.5 µM in 100 µL) for a total volume of

300 µL and incubated on a rotator at rt for 1 hour. Storage buffer (500 µL) was added and incubated with rotation at rt for 5 min to fill any remaining active sites on the beads with BSA. The beads were washed twice in 200 µL storage buffer, resuspended in 500 µL storage buffer, and stored at 4°C until used. The level of bead aggregation and protein binding was assessed by microscopy using rabbit-anti-V5-549 antibodies against the V5 tag on the rSpTrf proteins cross-linked to the beads. All wash steps were carried out with a magnet stand to collect the beads prior to removing the wash buffers.

2.6 Sea urchins

Adult sea urchins, *Strongylocentrotus purpuratus*, were purchased from the Southern California Sea Urchin Company (Corona del Mar, CA) after collection from the coast of southern California near San Diego. Sea urchins were fed rehydrated kelp (WEL-PAC) and maintained as described (50, 51).

2.7 Phagocytosis

CF was withdrawn from sea urchins as described (52) with 23 gauge needles attached to 1 ml syringes pre-loaded with 400 µl of CMFSW-EH to block clotting. Cells were dispensed into a 1.5 ml tube on ice containing 500 µL of CMFSW-EH and counted in a TC20 cell counter (BioRad).

2.7.1 rSpTrf::beads incubated with phagocytes spun onto slides

Coelomocytes (3.65 x 10^4 or 7.3 x 10^4 cells/mL) were centrifuged onto Shandon Superfrost Plus positively charged microscope slides (Thermo Scientific or Epredia) at 1000 x *g* for 5 min at 4°C using slide holder assemblies with dual cytology chimneys (18 mm diameter, Hettich Zentrifugen). The slides in the slide holder assemblies were incubated at 4°C for 5 min to allow the cells to spread, and then moved to 14°C for 10 min. The CMFSW-EH was replaced with coelomocyte culture medium [CCM; 0.5 M NaCl, 5 mM $MgCl_2$, 1 mM EGTA, 20 mM HEPES, pH 7.4 (37, 53)] every 10 min to 33%, 66%, 100% CCM as recommended (54). Two pipettes were used to aspirate CMSFW-EH and add CCM to ensure that the cells bound to the slide did not dehydrate. The cells were incubated at 14°C for 30 min, followed by replacing the CCM with rSpTrf::beads in CCM (100 beads/cell) and incubated for 20 min at 14°C. CCM (1 mL) was added to dilute and wash unbound beads from the cells, followed immediately by dismantling the slide holder assemblies. The cells were fixed for further processing and analysis (see below).

2.7.2 rSpTrf::beads blocked with anti-SpTrf antibodies

Beads cross-linked to rSpTrf-E1 or rSpTrf-E2-3 were blocked using a mixture of rabbit anti-natSpTrf-66, -68, and -71 [100X dilution (37)], or with normal rabbit serum (NRS; 100X dilution) as the controls. Deglycosylation of N-linked oligosaccharides of rSpTrf-E1::beads and rSpTrf-E2-3::beads was conducted as described above using PNGaseF (New England Biolabs). Deglycosylated rSpTrf-E1::beads and rSpTrf-E2-3::beads were blocked with anti-natSpTrf antibodies or NRS. Beads were first incubated in blocking buffer (BB-PBS; 3% bovine serum albumin [BSA], 3% normal goat serum [NGS] in PBS) for 45 min at rt with rotation followed by incubation with the antibodies or NRS in BB-PBS for 1 hr at rt with rotation. Beads were washed 3 times with PBS, resuspended in 300 µL of storage buffer (Bangs Laboratory) and stored at 4°C until used. Coelomocyte association with glycosylated and deglycosylated, blocked, and control rSpTrf-E1::beads and rSpTrf-E2-3::beads was assessed as described above. Briefly coelomocytes were spun onto slides, the buffer was changed to CCM, and the cells were incubated with beads for 20 min at 14°C. The cells were washed and fixed for further processing and analysis (see below).

2.7.3 rSpTrf::beads incubated with phagocytes in suspension

Beads cross-linked with proteins were washed with 200 µL artificial coelomic fluid [aCF; 10 mM $CaCl_2$, 14 mM KCl, 50 mM $MgCl_2$, 398 mM NaCl, 1.7 mM $NaHCO_3$, 25 mM Na_2SO_4, pH 7.4 (30)] and resuspended in 100 µL of aCF. Coelomocytes in CMFSW-EH (~1 mL) were pelleted at 5000 x *g* for 7 min at 4°C. The supernatant was discarded and the cells were resuspended in 400 µL of aCF using a 1 ml pipette in which the tip was cut 5 mm from the end using a sterile razor blade to increase the bore diameter and reduce shear stress while the pelleted cells were resuspended. Cells were counted on the TC20 (Bio-Rad) cell counter and 1 x 10^5 or 2 x 10^5 cells/ml were transferred to a 1.5 ml tube. The rSpTrf::beads in aCF were added to the cells and the volume was brought to 500 µL with aCF (50 beads/cell). The cells were incubated with beads for 40 min at 14°C with agitation every 10 min. The cells and beads were moved to a dual cytology chimney in a slide holder assembly with a Superfrost Plus Slide (Epredia) and incubated for 20 min at 14°C to allow cells to settle and adhere to the slide. Chimneys were centrifuged in a swinging bucket rotor at 18 x *g* for 10 min at 4°C. The slide holder assembly was dismantled, and the slides were transferred to a cold metal sheet on ice. Live cells were blocked on ice for 1 hr in 125 µL of blocking buffer in aCF (BB-aCF; 3% BSA, 3% NGS). BB-aCF was tipped off the slides and cells that had been incubated with rSpTrf::beads were incubated for 1 hr with rabbit-anti-V5-549 (1000X dilution in BB-aCF; Rockland) at 0°C. Cells that had been incubated with BSA::beads were incubated in parallel with rabbit-anti-BSA (5,000X dilution in BB-aCF; ThermoFisher). Slides were transferred into a Coplin jar containing ice cold aCF and incubated for 5 min to remove unbound antibodies. Cells were fixed, permeabilized, and processed as described below and incubated with mouse-anti-actin (1500X dilution; MP Biomedicals) followed by goat-anti-mouse-488 (6000X dilution; Invitrogen), and 4',6-diamidino-2-phenylindole (DAPI). Concurrently, cells treated with BSA::beads were also incubated with goat-anti-rabbit-555 (5000X dilution; Invitrogen). Manual counts of beads per cell were done blind with regard to which protein was cross-linked to the beads.

2.8 Phagocyte fixation, permeabilization, and immunofluorescence

Phagocytes bound to slides were fixed as described previously (37, 52). Cells were incubated in prefix (0.000025% glutaraldehyde in CCM or aCF) for 5 min at 14°C, fixed immediately without washing (2% formaldehyde, 0.25% Triton X-100) in AC320 buffer (320 mM sucrose, 75 mM KCl, 2 mM $MgCl_2$, 20 mM EGTA, 20 mM Pipes pH 7.4 (37, 53)) for 5 min at 14°C. Cells were permeabilized with ice cold methanol in a Coplin jar for 5 min at -20°C followed by a wash in PBS in a Coplin jar for 5 min at rt. Slides were moved to a humid chamber and cells were incubated with blocking buffer (BB-PBS; 3% BSA, 3% NGS in PBS) for 1 hr at rt followed by 3 washes in PBS for 5 min in a Coplin jar. To evaluate phagocytosis of beads by phagocytes spun onto slides, cells were incubated with rabbit-anti-V5-549 (3000X dilution in BB-PBS; Rockland) and mouse-anti-actin (1500X dilution in BB-PBS, MP Biomedicals) for 1 hr in a humid chamber followed by 3 washes in PBS of 5 min each in a Coplin jar. In parallel experiments to evaluate surface binding vs. phagocytosis of beads by phagocytes in suspension, cells were incubated with rabbit-anti-V5-549 at 0°C prior to fixation and were incubated with mouse anti actin after fixation and permeabilization, as described above. In the last step for all cytology protocols, cells were incubated with goat-anti-mouse-Ig-488 (6000X dilution in BB-PBS, Invitrogen) for 1 hr in a humid chamber. Cells were washed in PBS, and 10 µL of ProLong Gold antifade reagent with DAPI (Invitrogen) was added and a coverslip was added and sealed with clear nail polish. Cells were evaluated by fluorescence (Axioskop; Zeiss) and confocal (LSM 710; Zeiss) microscopy to quantify beads bound to the surface, beads phagocytosed, and the type of phagocyte was recorded.

2.9 Evaluation and statistics of phagocytes with beads

The data were visualized using boxplots to display both the mean and variability within each treatment group, to enable comparison between different experimental conditions. All visualizations and statistical analyses were conducted in R (version 4.3.0).

The association of beads per phagocyte for spun cells was determined by visual inspection using fluorescence microscopy (Axioskop; Zeiss). For each slide, 500 phagocytes per animal were evaluated, and cells from a minimum of six different sea urchins were used to evaluate each of the different proteins cross-linked to beads. The average number of beads associated with cells, and the percentage of phagocytes associated with at least one bead were evaluated. A Tukey ANOVA test was used to assess significant differences in the average number of phagocytes associated with beads cross-linked to different proteins.

Surface binding and phagocytosis of beads per phagocyte incubated in suspension, in addition to the type of phagocyte (polygonal, discoidal, or small) with beads was evaluated based on visual inspection by confocal microscopy (LSM 710; Zeiss). A minimum of 100 phagocytes per sea urchin were counted, and cells from a minimum of six sea urchins were evaluated for each protein. A Tukey ANOVA test was used to assess whether the average number of surface bound, and phagocytosed beads were significantly different among the different rSpTrf::beads. BSA::beads were used as the negative control. Data were also evaluated with a Dunnet test to identify significant differences between each of the rSpTrf::beads (treatment group) and the BSA::beads (control group). A two tailed paired *t*-test was used to evaluate significance between surface bound beads and phagocytosed beads for each protein cross-linked to beads.

2.10 Scanning electron microscopy

Based on methods described above, coelomocytes (10^5 cells) were either i) spun onto a circular cover slip (18 mm; Fisherbrand item # 12-546) and incubated with rSpTrf-E2-3::beads in aCF, or ii) incubated with rSpTrf-E2-3::beads in solution in aCF followed by spinning onto the circular cover slips. Cells centrifuged onto the coverslips used the dual cytology chimneys with the same diameter as the coverslip. For both methods coelomocytes were incubated with 100 beads per cell for 1 hr followed by fixation for SEM. Coelomocytes were incubated in prefix solution (0.001% glutaraldehyde in aCF (52)) for 5 min at 14°C followed by the fixative solution (2.5% glutaraldehyde, 1% paraformaldehyde, in AC320) for 30 min at rt. Cover slips were washed 3 times with 0.12 mM sodium cacodylate buffer pH 7.4 (Electron Microscopy Sciences) for 10 min with shaking. The coelomocytes were transferred to the post-fixation solution (1% OsO_4, 0.12 mM sodium cacodylate buffer, pH 7.4) for 1 hr at rt with shaking followed by 4 washes with deionized (DI) water for 10 min at rt. Dehydration was achieved by sequential immersion in ethanol at increasing concentrations (15%, 35%, 50%, 70%, 80%, 95%, 100%) for 10 min each at rt with shaking. Coverslips were submerged in hexamethyldisilane (HMDS) for 15 min at rt, moved into fresh HMDS, and incubated at rt overnight allowing for HMDS evaporation. Coelomocytes were sputter coated (Cressington 208HR Sputter Coater) with 2 nm PtPd and imaged with a scanning electron microscope (FEI Teneo LV SEM).

3 Results

3.1 rSpTrf proteins are expressed by Sf9 insect cells

Our prior attempts to express rSpTrf proteins in *E. coli* culminated in a single version, rSpTrf-E1-Ec (originally called Sp0032), that was expressed and isolated successfully (35). Other rSpTrf expression constructs failed presumably because the proteins were lethal to *E. coli*. Although our previous studies provided information about the functions of rSpTrf-E1-Ec, questions remained regarding the functions of other versions, which were proposed to be different and perhaps complementary (35). Because of the toxicity of expressing rSpTrf proteins in *E. coli*, eukaryote cells were chosen for recombinant protein expression. Six distinct versions of SpTrf proteins were expressed in Sf9 insect cells that

were selected based on size, sequence diversity, expression level (30) (Figure 1), as well as to compare the functions of rSpTrf-E1 to rSpTrf-E1-Ec. The choice of proteins included rSpTrf-01, -E1, -C1, -D1, and -A6 that were based on element pattern, in addition to rSpTrf-E2 and a variant called rSpTrf-E2.1, which show the highest expression level in coelomocytes (30). The rSpTrf proteins isolated from the cell cultures were initially evaluated by protein gels and Western blots to determine the molecular weights and expression levels, which showed that six constructs yielded recombinant proteins (Figures 2A, B). However, rSpTrf-E2.1, a truncated version of rSpTrf-E2, was not produced and secreted by the Sf9 cells even though the expression vector was incorporated into the genome of the cells and was transcribed (Supplementary Text File 1). Consequently, rSpTrf-E2.1 was not investigated further.

The six rSpTrf proteins ranged in molecular weight upon isolation from ~40 kDa to ~65 kDa (Figures 2A, B). However, two different isolations of rSpTrf-E2 resulted in proteins of different molecular weights (Table 1). A preliminary isolation of rSpTrf-E2 (denoted as rSpTrf-E2-4) was ~45 kDa, which was smaller than rSpTrf-A6, -D1, and -C1 (Supplementary Figure S3A). However, after a second large-scale isolation and storage, rSpTrf-E2-4 appeared on Western blots at ~80 kDa (Table 1; Supplementary Figure S3B), suggesting dimerization. In a different large-scale isolation of rSpTrf-E2 (denoted as rSpTrf-E2-3), it remained at 45 to 50 kDa over time (Table 1). Because the expression constructs for rSpTrf-E2-3 and rSpTrf-E2-4 included the identical SpTrf sequence, although with different ligation methods, the amino acid sequences of these two rSpTrf-E2 isolates were essentially identical. Although we cannot speculate as to why rSpTrf-E2-4 dimerized while rSpTrf-E2-3 did not, this difference provided an opportunity to test the functions of a dimerized compared to a non-dimerized version. This was particularly noteworthy given that dimerized rSpTrf-E1-Ec is not functional compared to the monomer (40).

When CF is collected from any sea urchin species, the native Trf proteins are mostly multimerized with only a few proteins within the expected size range of monomers (25, 26, 37, 43). To determine whether the rSpTrf proteins would multimerize with each other, rSpTrf-E2-3 and rSpTrf-E1 were mixed in equal mass with each of the other proteins and evaluated for multimerization based on size change on Western blots. However, results showed that the protein mixtures did not show increased band sizes on Western blots suggesting that multimers did not form (Supplementary Figure S4).

3.2 All of the rSpTrf proteins are glycosylated

The molecular weight of rSpTrf-E1-Ec deduced from Western blots matches the molecular weight deduced from the cDNA sequence (35). However, all of the rSpTrf proteins isolated from Sf9 cells were larger than predicted (Figures 2A, B; Table 1). Evaluation of the amino acid sequences of each rSpTrf protein predicted that each had numerous conserved sequence motifs for

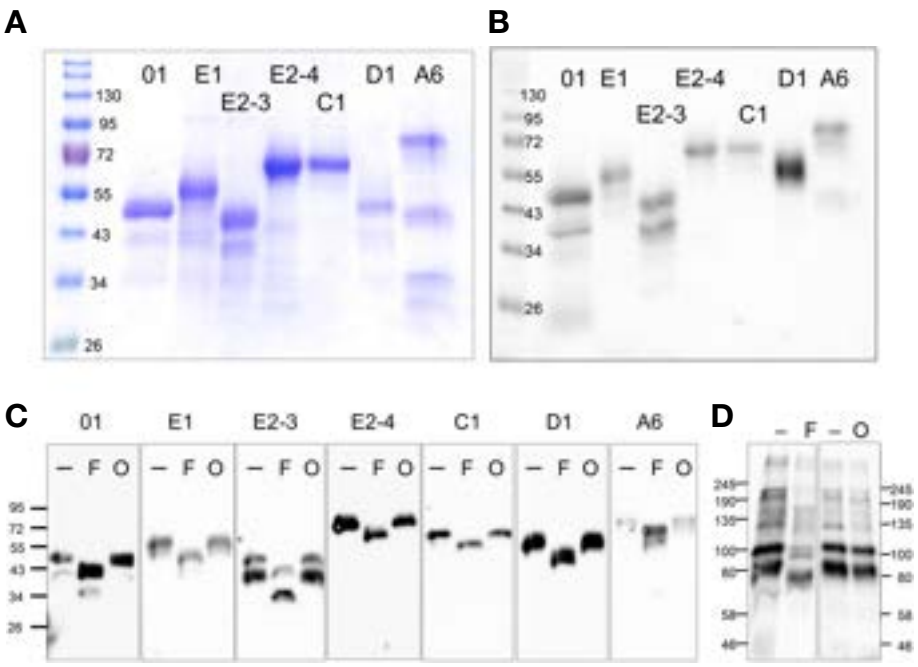

FIGURE 2
rSpTrf proteins are expressed in Sf9 insect cell cultures. **(A)** A Coomassie stained protein gel shows the rSpTrf proteins isolated from insect cells. **(B)** A Western blot shows the rSpTrf protein bands are based on recognition by rabbit-anti-V5-HRP. Broad Range protein standards (BioRad) are shown on the left. **(C)** The rSpTrf proteins are glycosylated with N-linked oligosaccharides. Each of the proteins was incubated with PNGaseF (F) to remove N-linked oligosaccharides, and a combination of neuraminidase and *O*-glycosidase (O) to remove O-linked oligosaccharides. Size changes were identified based on comparison to untreated controls (-). **(D)** CF containing natSpTrf proteins was treated with the glycosidases, which shows size changes with PNGaseF (F), but not with neuraminidase and *O*-glycosidase (O), compared to untreated controls (-). Rabbit-anti-natSpTrf antibodies (37) identify the natSpTrf proteins in the CF.

post-translational glycosylation (Table 1; Supplementary Table S1) (30). The rSpTrf proteins were evaluated for both N-linked and O-linked glycosylation by incubation with deglycosidases followed by Western blots to evaluate size changes. When the rSpTrf proteins and natSpTrf proteins were incubated with peptide N-glycosidase F (PNGaseF), *O*-glycosidase alone, or *O*-glycosidase plus neuraminidase A, proteins only decreased in size after treatment with PNGaseF compared to untreated controls (Figure 2C). However, the reduced sizes did not match the deduced sizes based on gene and transcript sequences. The combination of *O*-glycosidase with or without neuraminidase A did not alter the sizes of the proteins even though conserved motifs for O-linked oligosaccharides have been predicted (Figure 2C) (30, 33). However, the Sf9 cells likely did not add complex O-linked oligosaccharides to the rSpTrf proteins (55). Similar results were obtained for natSpTrf proteins after treatment with *O*-glycosidase (Figure 2D). This suggested that the recombinant and native natSpTrf proteins were only glycosylated with N-linked oligosaccharides. The analysis did not address the possibility that the proteins may have had O-linked oligosaccharides that were not removed by the *O*-glycosidase treatment. Whether the increased molecular weight of the rSpTrf proteins was due to other post-translational modifications or associations with other unknown molecules was not addressed.

3.3 rSpTrf::beads show augmented association with phagocytes

Previous analysis of rSpTrf-E1-Ec reported that it bound to *Vibrio diazotrophicus* in addition to *Vibrio* flagellin (35), however it did not augment phagocytosis of opsonized *V. diazotrophicus* by phagocytes (38). In comparison, natSpTrf proteins isolated from cfCF by nickel affinity opsonized *V. diazotrophicus* and augmented phagocytosis by phagocytes. Consequently, it was postulated that the natSpTrf-E1 isoform may interact with other versions during the opsonization and phagocytosis of foreign particles and microbes and that other natSpTrf proteins had different but overlapping functions (35, 36, 38). Because the expression of other rSpTrf proteins from *E. coli* failed, this possibility was not addressed. With the expression of several rSpTrf proteins from insect cells, the hypothesis was tested using rSpTrf proteins bound to inert beads. The use of inert beads removed the confounding effects of surface PAMPS on bacteria, such as LPS, that are detected by sea urchin cells (56–60), induce the expression of the *SpTrf* gene family (30), and likely drive phagocytosis of Gram negative bacteria (38). The use of rSpTrf::beads limited the interactions between the cells and beads exclusively to the phagocyte cell surface and the rSpTrf proteins. Initial analyses of phagocytosis employed magnet capture of phagocytes that had taken up magnefy beads. However, results showed significant background using coelomocytes with this approach (Supplementary Text File 2). Consequently, opsonin function of rSpTrf proteins was inferred from phagocytosis of rSpTrf::beads by phagocytes spun onto slides followed by visual inspection using microscopy. The percentage of phagocytes associated with rSpTrf::beads was significantly ($p < 0.05$) higher compared to BSA::beads, which served as the negative control (Figure 3A).

Because there were no significant differences in the percentages of phagocytes associated with different rSpTrf::beads, this suggested that the phagocytes had comparable binding for the different rSpTrf proteins. However, these results did not verify specific interactions that occurred directly between the rSpTrf::beads and the phagocytes. To address this, three rabbit-anti-natSpTrf antibodies [see Supplementary Figure S2 that shows the peptide sequences to which the antibodies were raised and their locations in the proteins; see also (37)] were incubated with rSpTrf-E1::beads and rSpTrf-E2-3::beads prior to mixing with the cells. rSpTrf-E1 and -E2-3 were chosen because they had the lowest and highest percent association with phagocytes, respectively (Figure 3A). This was done to determine whether the antibodies bound to the rSpTrf::beads would interfere with the association between the rSpTrf proteins and the phagocytes. Results showed a significant reduction in the association of rSpTrf-E1::beads with cells, suggesting a specific interaction between rSpTrf-E1 and the phagocytes (Figure 3A). However, the anti-SpTrf antibodies did not reduce the association between the rSpTrf-E2-3::beads and the phagocytes. To determine whether the N-linked oligosaccharides were blocking antibody access to one or more of the binding sides on the proteins, both rSpTrf-E1::beads and rSpTrf-E2-3::beads were deglycosylated with PNGaseF prior to repeating the experiment. Results showed that the anti-natSpTrf antibodies reduced the association of both deglycosylated rSpTrf-E1::beads and rSpTrf-E2-3::beads with phagocytes compared to the glycosylated proteins (Figure 3C). However, deglycosylation also decreased general bead association with the phagocytes when the antibodies were not used for blocking (compare Figures 3B, C). These findings suggested that the interactions between rSpTrf::beads and the phagocytes was specific rather than constitutive, non-specific binding to foreign particles. This specificity is in agreement with a similar result for PlTrf proteins in the sea urchin, *Paracentrotus lividus* (26).

3.4 Phagocytes spun onto slides are incapable of internalizing beads

Based on the initial evaluation by standard microcopy, it was not possible to discern whether the rSpTrf::beads had been phagocytosed or whether they were only bound to the surface of the cells. To test this, phagocytes spun on slides were incubated with rSpTrf::beads, then moved to 0°C and incubated with a rabbit-anti-V5-549 antibody before fixation and permeabilization. This limited the binding of the anti-V5-549 antibody to rSpTrf::beads that were on the surface of the phagocytes and any beads that had been phagocytosed were inaccessible by the antibody. This approach showed that all beads associated with the phagocytes had bound the antibody and appeared red suggesting that all were surface bound and none were internalized (Figures 4A-D). Z-stack evaluation by confocal microscopy confirmed that the rSpTrf::beads were not phagocytosed and that they were consistently located above the actin cytoskeleton, suggesting that they were surface bound (Figure 4E). The approach that blocked antibody penetration into

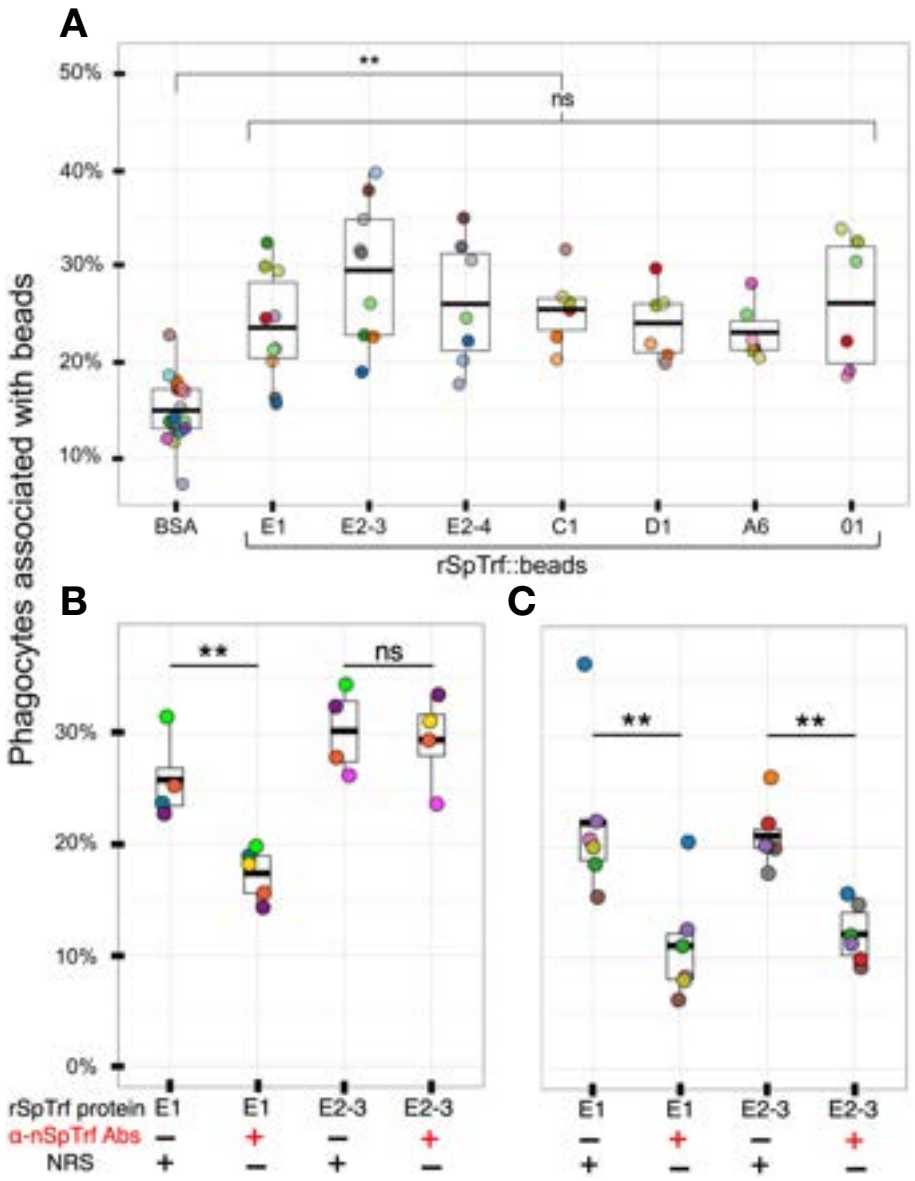

FIGURE 3
All rSpTrf proteins cross-linked to beads augment the association with phagocytes. **(A)** When phagocytes bound to slides are incubated with rSpTrf::beads, a greater percentage of phagocytes (**, $p < 0.05$) are associated with beads compared to the control BSA::beads. There are no significant differences (ns) among the rSpTrf proteins relative to the association of beads with phagocytes. **(B)** Pre-incubation of rSpTrf-E1::beads and rSpTrf-E2-3::beads with three rabbit-anti-natSpTrf antibodies reduces the percentage of phagocytes associated with rSpTrf-E1::beads (**, $p < 0.05$), but has no significant effect on rSpTrf-E2-3::beads (ns). **(C)** Deglycosylation of the rSpTrf::beads prior to blocking with rabbit-anti-natSpTrf antibodies decreases (**, $p < 0.05$) the percentage of phagocytes with associated rSpTrf-E1::beads and rSpTrf-E2-3::beads compared to beads that are not pre-incubated with the antibodies. Each dot represents the results for phagocytes collected from a single sea urchin. For each protein at least six animals were tested, and at least 500 cells per animal were counted for bead association. The protease inhibitor, HALT (1%), was added to all proteins. The box plots show the average and interquartile range of each bead treatment associated with phagocytes. A Tukey ANOVA test was used to evaluate the significance in bead association among cells incubated with the different rSpTrf proteins cross-linked to beads.

the cytosol prior to fixation and permeabilization was confirmed with a mouse-anti-actin. The absence of cytoskeletal labeling indicated that the antibody was blocked from crossing the cell membrane (Supplementary Figure S5).

To further verify that beads were limited to the surface of phagocytes and not internalized, scanning electron microscopy was used to visualize the phagocyte interactions with rSpTrf-E2-3::beads. This rSpTrf protein was chosen because it showed the highest average percentage of cells with beads on the surface (Figure 3A). The SEM images suggested that spun cells were able to recognize the rSpTrf-E2-3::beads because the number of beads on the cell surface (n = 7; the cell was 22% of the area in the field of view) was generally higher than the number of beads on the glass slide (n = 5; 78% of the area) (Figures 4F, G; Supplementary Figure S6). However, the morphology of the spun cells suggested that they were spread too thinly to take up the 1 µm beads that were bound to the surface.

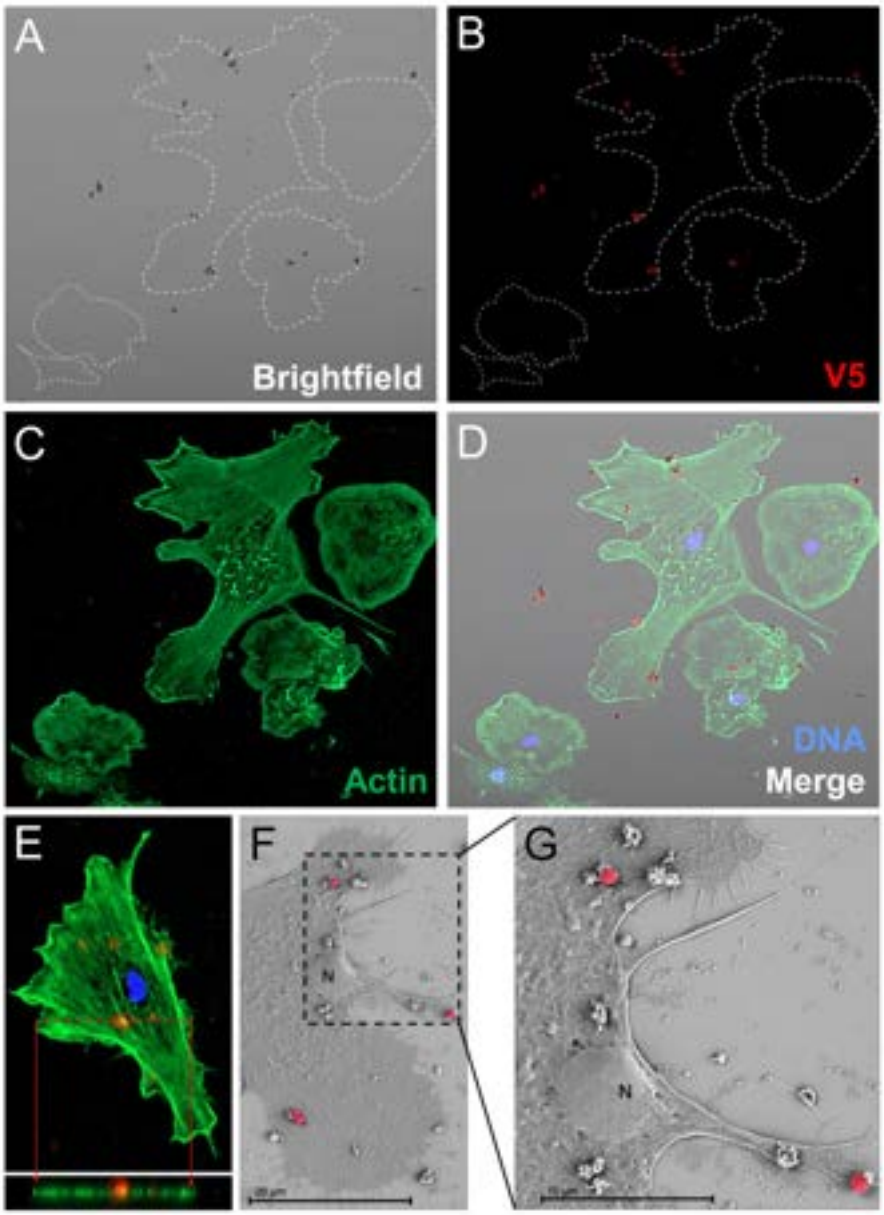

FIGURE 4
Phagocytes spun onto glass slides prior to incubation with rSpTrf::beads do not phagocytose surface bound beads. Spun cells with associated beads were incubated with rabbit-anti-V5-549 at 0°C followed by fixation and permeabilization for mouse-anti-actin and goat-anti-mouse-Ig-488 incubation. All beads were bound by rabbit-anti-V5-549 and appear red identifying only surface bound beads. No unlabeled beads are identified indicating that none are phagocytosed. **(A)** Bright field shows the location of all beads. **(B)** rSpTrf::beads are identified by rabbit-anti-V5-549 by UV epifluorescence. **(C)** Actin labeling of the cytoskeleton defines the types of phagocytes in the field; polygonal (P) and discoidal (D) phagocytes. **(D)** The merged image shows that all beads are labeled red indicating that no beads are internalized. **(E)** A Z-stack analysis by confocal microscopy shows that all beads are positioned above the cell surface and that none are positioned within the actin cytoskeleton. This indicates that the rSpTrf::beads are only surface bound. The DNA is labeled with DAPI. **(F, G)** Scanning electron microscopy confirms that spun phagocytes do not take up surface bound rSpTrf-E2-3::beads (false red color). Spun phagocytes are extremely flat, which decreases the vertical cytosolic space so that 1 µm beads are not internalized. The comparison between the beads bound to the cell surface vs. those bound to the slide surface suggests cellular recognition of rSpTrf-E2-3::beads.

3.5 Phagocytes bind and internalize rSpTrf::beads when incubated in solution

To address the inability of spun and flattened phagocytes to take up the rSpTrf::beads, the approach for incubating the cells with the rSpTrf::beads was modified. Cells were incubated with the beads in solution, followed by a low-speed spin onto slides. As above, cells held at 0°C on slides were incubated with the rabbit-anti-V5 antibody prior to fixation and permeabilization to identify the beads on the surface vs. those that had been phagocytosed and were unavailable to the antibody. Results showed that in addition to binding beads on the surface, phagocytes also internalized the rSpTrf::beads when

incubated in solution (Figure 5; Supplementary Figure S7). Different rSpTrf::beads showed differences in both surface binding and phagocytosis with variations in the number of beads per phagocyte (Figure 6A). There were more rSpTrf-E2-3::beads bound to the surface of cells, and results for the other rSpTrf::beads revealed several levels of binding to cell surfaces (Table 2). There were more phagocytosed rSpTrf-E2-4::beads per cell compared to the other rSpTrf::beads (Figure 6B). Furthermore, the numbers of phagocytosed beads per cell were slightly different than the number of surface beads per cell. These findings suggested that phagocytes could recognize rSpTrf-E2-3, -A6, -01 and -E2-4 cross-linked to beads, whereas binding and uptake of beads cross-linked to rSpTrf-E1, -C1, and -D1 were not different from the control BSA::beads (Table 2).

When the results for beads per phagocyte were re-evaluated as the percentage of phagocytes associated with at least one bead, similar results were obtained relative to the rSpTrf protein cross-linked to the beads (Figure 7A). There were significantly more phagocytes associated with beads cross-linked to rSpTrf-E2-3, -E2-4, -A6, -01, and -C1 compared to beads cross-linked to rSpTrf-E1, -D1, and -BSA. However, the results for rSpTrf-C1::beads were different; there were significantly more cells associated with at least one rSpTrf-C1::bead compared to the number of C1::beads per phagocyte (compare Figures 7A, 6A, B). When the number of rSpTrf::beads per cell on the surface was compared to those phagocytosed for the same rSpTrf protein, results generally showed significantly fewer beads inside the cells compared to those on the surface (Figure 6C). However, this did not apply to rSpTrf-E2-4::beads and rSpTrf-A6::beads, which showed similar numbers of beads bound to the surface and those phagocytosed. When cells collected from different sea urchins were evaluated, differences in the recognition of the same rSpTrf protein among the animals were observed (Figure 7B). The average number of phagocytes associated with rSpTrf::beads was variable and ranged from 53% (sea urchin 4 and rSp-Trf-E1) to 92% (sea urchin 8 and rSpTrf-E2-3). Although for cells from other sea urchins (*e.g.*, 6 and 7) similar numbers of phagocytes (75%) were associated with at least one bead cross-linked to rSpTrf-E1, -E2-4, and -01. Overall, these findings suggested that phagocytes showed specific recognition of certain rSpTrf proteins cross-linked to the beads.

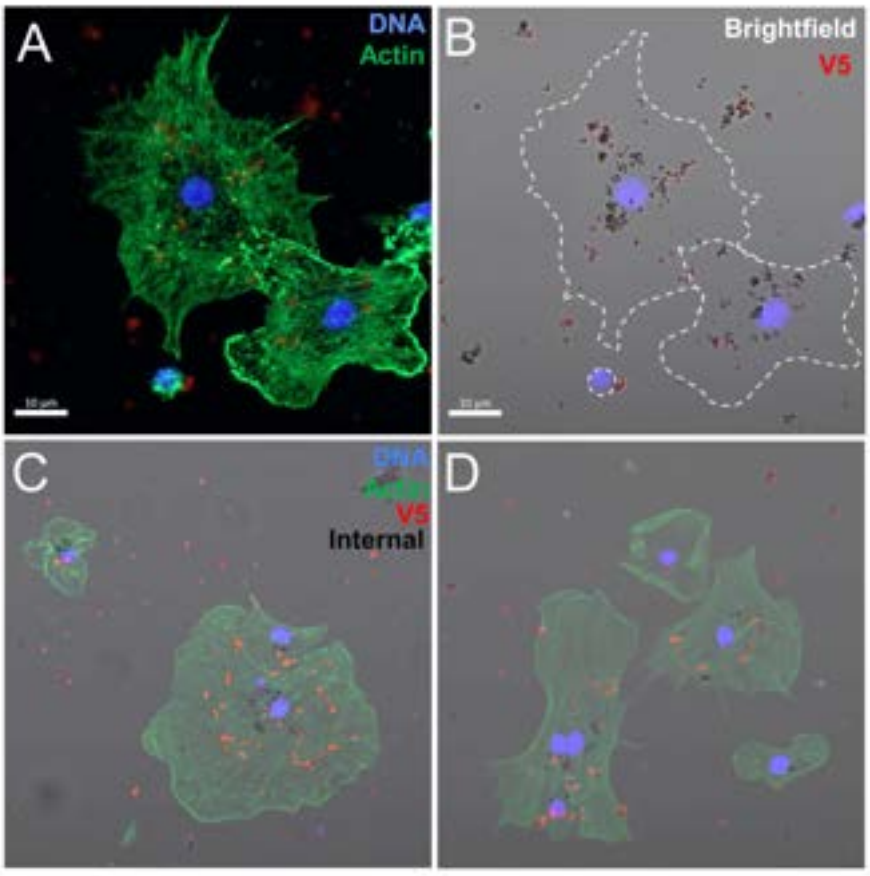

FIGURE 5
Coelomocytes incubated with rSpTrf-E2-3:beads in solution result in bead phagocytosis. When coelomocytes are incubated with beads in solution, they are capable of phagocytosis. Beads on the outside of the cells are labeled with rabbit-anti-V5-549 (red) before fixation and permeabilization, which blocks antibody access to the internalized beads (black). **(A, B)** Two polygonal phagocytes take up rSpTrf-E2-3::beads. The bright field image shows red beads that are located on the cell surface and unlabeled black beads that are phagocytosed. **(C, D)** Merged images show phagocytes with red beads on the surface and black beads that have been phagocytosed.

10.3389/fimmu.2024.1372904

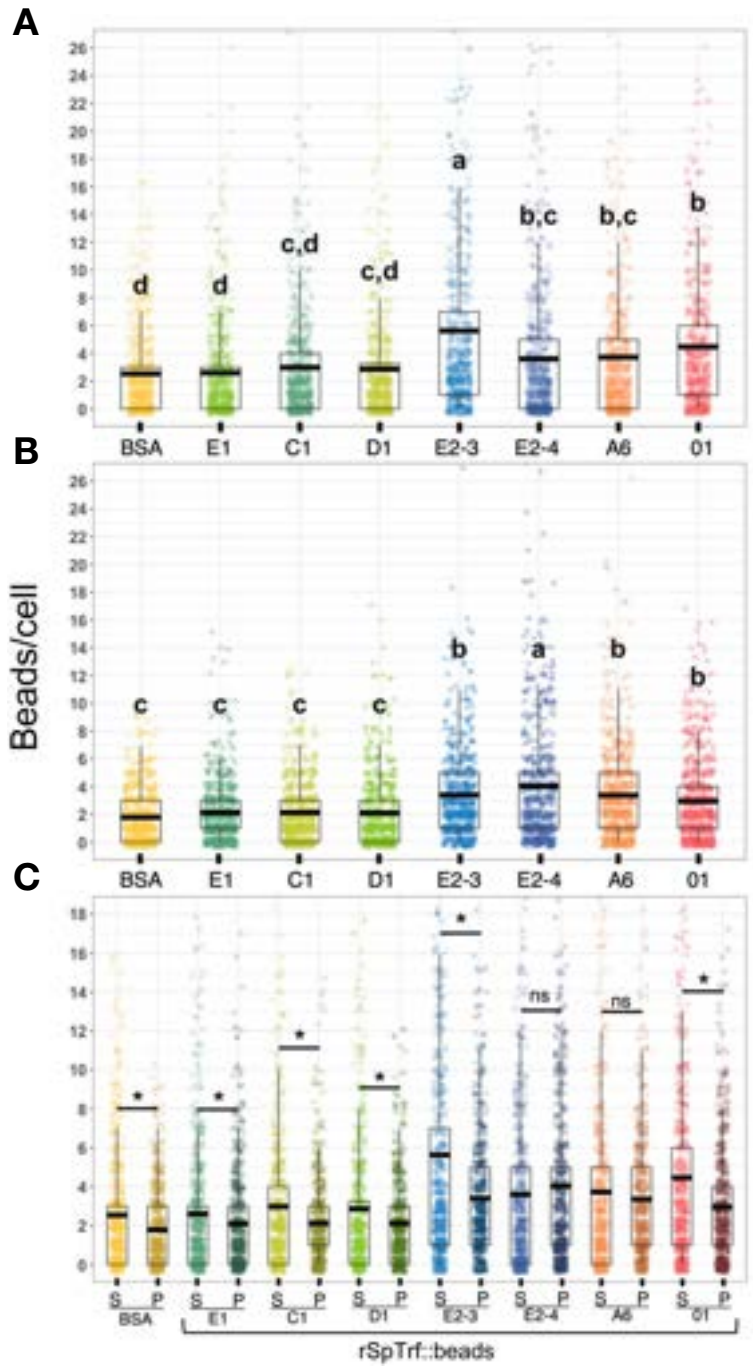

FIGURE 6
The rSpTrf::beads show significant differences in the number of beads bound and phagocytosed by phagocytes. The numbers of beads per cell were evaluated for phagocytes based on beads bound to the cell surface and beads phagocytosed. The box plots show the average and interquartile range of each rSpTrf::bead treatment associated with phagocytes. **(A)** Differences in the number of rSpTrf::beads bound to the cell surface is based on the rSpTrf protein. **(B)** Differences in the number of phagocytosed rSpTrf::beads by phagocytes resolves to those with specific phagocytosis and those that are not different from the control BSA::beads. Data analysis was based on a total of 600 cells counted for each rSpTrf::bead and cells collected from six different sea urchins. Statistical analysis employed Tukey ANOVA and significance was set to $p < 0.05$. The letters above the boxplots indicate significant differences or similarities among groups. See also Table 2 for the different levels of binding and phagocytosis of the rSpTrf::beads based on statistical results using the Dunnet test. **(C)** The number of surface bound beads (S) compared to the number of phagocytosed beads (P) shows, for most proteins, that there are significantly more rSpTrf::beads bound to the cell surface than are phagocytosed (*, paired *t*-test, $p < 0.05$). There are no significant differences (ns) between surface bound and phagocytosed rSpTrf-E2-4::beads and rSpTrf-A6::beads.

Some rSpTrf proteins enhanced bead binding and internalization by phagocytes, whereas others showed patterns similar to those of the control beads.

3.6 Polygonal phagocytes are the major phagocyte for recognition and uptake of rSpTrf::beads

The coelomocytes of the phagocyte class of cells in the purple sea urchin have been characterized based on their numbers in the CF, their cytoskeletal morphology, and differences in size ((53, 61, 62); reviewed in (63, 64)). These colorless, filopodial or lamellipodial cells bind tightly to glass and are phagocytic (37, 65, 66), even though this has not been tested for small phagocytes (39). By discriminating polygonal, discoidal, and small phagocytes based on their distinct morphologies and sizes, these cell subsets were compared for surface binding and phagocytosis of the SpTrf::beads. Medium phagocytes were not identified and may only appear in response to loss of CF (39). Results showed that all three types of phagocytes bound and phagocytosed the rSpTrf::beads (Figure 8). The polygonal phagocytes associated with the most rSpTrf::beads and showed two levels of binding and phagocytosis of the several rSpTrf proteins cross-linked to the beads (Figures 9A, B; Table 2). There were significantly more rSpTrf-E2-3::beads bound to the cell surfaces, and an intermediate level of beads cross-linked with rSpTrf-E2-4, -A6, and -01 (Figure 9A). Surface binding of rSpTrf–E1, –C1, and –D1 were not different from the BSA::beads. Polygonal phagocytes internalized more rSpTrf-E2-4::beads (Figure 9B) with some differences in phagocytosis of the other rSpTrf::beads compared to those bound to the surface (Table 2). In general, the rSpTrf-E2::beads showed the greatest number of beads bound to the surface and internalized by polygonal phagocytes. In contrast, the discoidal cells bound and phagocytosed rSpTrf::beads (Figures 8C, D), but quantification indicated that the interactions were either not different from the BSA::beads (Figures 9C, D) or that there were low levels of binding or phagocytosis of rSpTrf-01 and -C1 cross-linked to beads (Table 2). Consequently, the discoidal cells demonstrated low levels of base-line, constitutive binding and phagocytosis of rSpTrf::beads without distinction among the rSpTrf proteins. It is noteworthy that while the discoidal phagocytes did not differentiate among the various rSpTrf::beads and the BSA::beads, they exhibited a comparable number of bound and phagocytosed BSA::beads as the polygonal phagocytes (compare Figures 9A, B with C, D). This suggested that the discoidal and polygonal phagocytes exhibited similar levels of constitutive phagocytosis.

Small phagocytes have been identified more recently (37, 50) than the large phagocytes and therefore little is known about their functions, including whether these cells are capable of phagocytosis. Imaging of small phagocytes illustrated their capabilities for binding and phagocytosis of rSpTrf::beads (Figures 8E, F). These small cells showed elevated binding for beads cross-linked with rSpTrf-E2-3, -A6, and -01, whereas the remaining rSpTrf::beads were not different from the BSA::beads (Figure 9E; Table 2). Small phagocytes internalized rSpTrf-E2-4::beads more readily than the other rSpTrf proteins (Figure 9F; Table 2). These results demonstrated that these small phagocytes were capable of taking up multiple beads. Overall, these findings showed that the three types of phagocytes functioned differently for binding and phagocytosis that ranged from specific associations with specific rSpTrf::beads to non-specific, constitutive phagocytosis. The polygonal phagocytes appeared as the major phagocytic cell in sea urchins.

4 Discussion

Expanded gene families encoding immune response proteins are present in a wide variety of invertebrates and are a basic attribute of innate immunity in these animals. Examples include the *C1q* gene family in the oyster, *Crassostrea gigas* (67, 68), the gene family encoding the fibrinogen related proteins (FREPs) in molluscs (69), the gene family encoding the variable chitin binding proteins (VCBPs) in amphioxus, *Branchiostoma floridae* (70), several gene

TABLE 2 Different types of phagocytes and different rSpTrf::beads show different levels of binding and phagocytosis[1].

Cell type	Bead location	Level of binding and phagocytosis of rSpTrf::beads[2]			
		High	Medium	Low	ns
All phagocyte types	Surface Bound	E2-3, A6, 01	E2-4		E1, C1, D1
	Phagocytosed	E2-4, E2-3, A6, 01			E1, C1, D1
Polygonal	Surface Bound	E2-4, E2-3, A6, 01			E1, C1, D1
	Phagocytosed	E2-4, E2-3, A6, 01	E1	C1	D1
Discoidal	Surface Bound			01	E2-4, E2-3, A6, E1, C1, D1
	Phagocytosed			C1	E2-4, E2-3, A6, 01, E1, D1
Small	Surface Bound	E2-3			A6, 01, E2-4, E1, C1, D1
	Phagocytosed		E2-4	E2-3	A6, 01, E1, C1, D1

[1]These results are also shown in Figures 7, 8, and as quantified in Figure 9 in which the data are evaluated by the Tukey ANOVA test.
[2]Significant differences in the number of rSpTrf::beads per cell compared to BSA::beads is based on the Dunnet test. High, $p \leq 0.001$; medium, $p \leq 0.01$; low, $p \leq 0.05$; ns, not significantly different from the control BSA::beads.

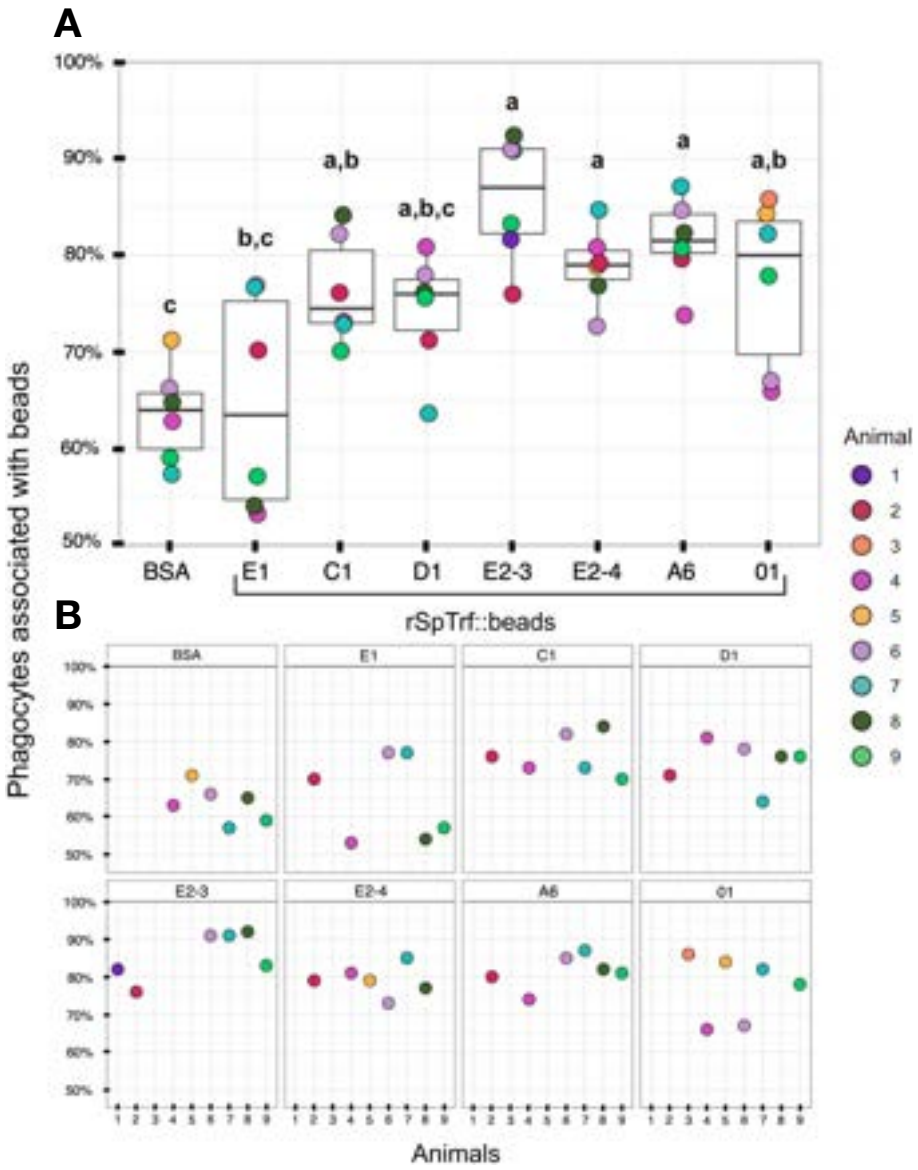

FIGURE 7
More phagocytes are associated with a subset of rSpTrf::beads compared to the control BSA::beads. Beads cross-linked to rSpTrf-E2-3, -E2-4, -A6, -C1, and -01 are associated with significantly more phagocytes ($p < 0.05$) than beads cross-linked with rSpTrf-D1, -E1, and the BSA control. **(A)** The box plots show the average and interquartile ranges for the average percentage of phagocytes with at least one bound or phagocytosed bead for the different rSpTrf::beads tested. Each dot represents the results for phagocytes collected from a single sea urchin. For each rSpTrf::bead, cells from at least six animals were tested, and at least 100 cells per animal were counted for bead association. Statistical analysis employed Tukey ANOVA and significance was set to $p < 0.05$. The letters above the boxplots indicate significant differences or similarities among groups. **(B)** The percentage of phagocytes with at least one bead shows variations among individual sea urchins. Cells from some animals were tested with subsets of rSpTrf::beads. Dots missing for individual animals indicate treatments that were not carried out for that animal.

families encoding AMPs in the housefly, *Musca domestica* (17), and the *SpTrf* gene family in euechinoids (24). The significant sequence diversity among the *SpTrf* genes, their expression patterns in response to immune challenge, and the functions of rSpTrf-E1-Ec for binding *Vibrio diazotrophicus* and PAMPs has established this system as an essential part of immune responses in sea urchins (reviewed in (24)). Here we extend these investigations to understand the functions of other rSpTrf proteins expressed by insect cell cultures. All of the rSpTrf::beads associated with significantly more phagocytes that were spun and flattened than control BSA::beads, suggesting that phagocytes have a cell surface mechanism for recognizing and binding the rSpTrf proteins. A subset of these proteins mediate binding of inert beads to phagocyte surfaces when cells are incubated in suspension, which enables them to phagocytose bound beads. Furthermore, the type of phagocyte that interacts with the bead shows variations in this process. The rSpTrf-E2 proteins show the highest level of binding to and phagocytosis by polygonal and small phagocytes. This is noteworthy because *SpTrf* genes encoding proteins with the E2 element pattern are the most highly expressed members of the gene family in response to immune challenges (29, 30) even though they are not the most numerous members of the family (31). However, gene expression level and

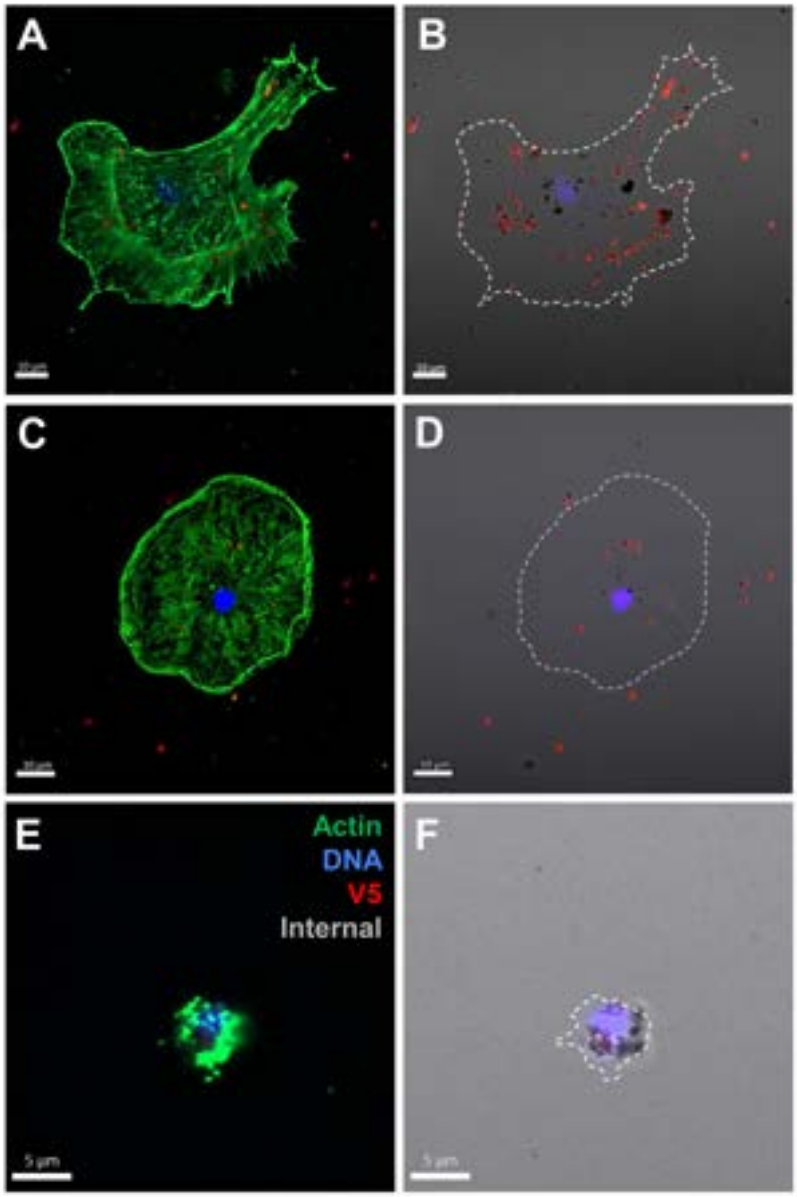

FIGURE 8
Polygonal, discoidal, and small phagocytes bind and phagocytose rSpTrf-E2-3::beads. Cells incubated with rabbit-anti-V5-549 prior to permeabilization labeled the beads bound to the cell surfaces, whereas internalized beads were not labeled because the antibodies were blocked from penetrating the plasma membrane. Identification of phagocyte type relied on actin cytoskeleton organization and cell size (37, 53). A polygonal cell **(A, B)** and a discoidal cell **(C, D)** have beads on the surface (red) as well as internalized beads (black). A small phagocyte **(E, F)** is also capable of bead phagocytosis showing unlabeled black beads around the nucleus.

binding function does not correlate for the other SpTrf proteins. The third highest expressed genes are those that encode SpTrf-C1, however these proteins do not show elevated binding functions (30). Alternatively, the *SpTrf-A* genes have very low expression, whereas the rSpTrf-A6 protein shows elevated binding. The rSpTrf proteins show several levels of binding and phagocytosis with some that do not support binding and phagocytosis above the constitutive level of the control BSA::beads. When these results are applied to the functions of the sea urchin immune system, they support the notion that different natSpTrf proteins have different functions, including acting indirectly as partners in opsonization (35, 36, 38) and perhaps in immune functions other than opsonization, although the rSpTrf proteins reported here were not tested for anti-bacterial activity.

4.1 Protein stability, dimerization, and function correlate with glycosylation

rSpTrf-E1-Ec shows both functional similarities and differences compared to the rSpTrf proteins expressed in insect cells. rSpTrf-E1-Ec binds to *Vibrio diazotrophicus*, but does not augment phagocytosis by phagocytes above base-line (38). Similarly, rSpTrf-E1::beads bind to

10.3389/fimmu.2024.1372904

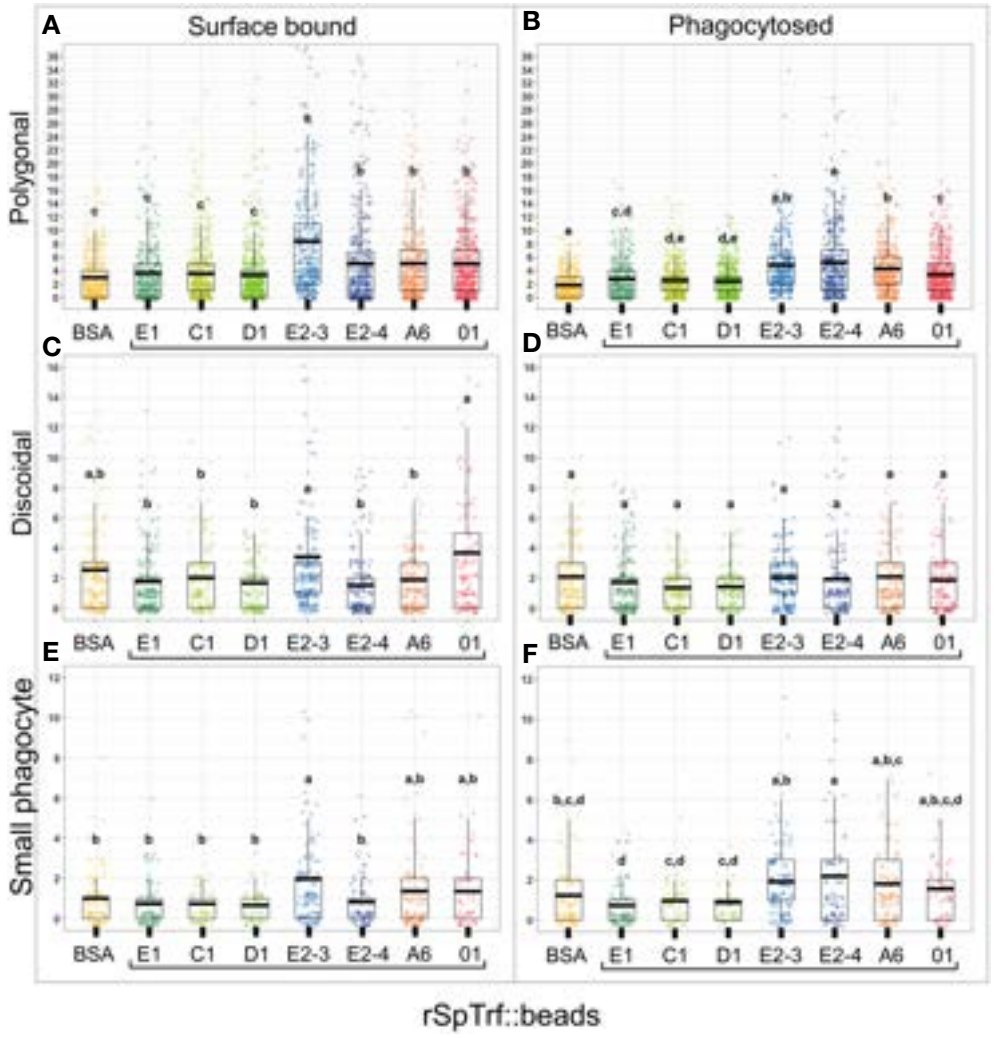

FIGURE 9
Different types of phagocytes show differences in binding and phagocytosis of rSpTrf::beads. Differential cell counts of cells processed for rabbit-anti-V5-459 labeling, as shown in Figure 8, are quantified for binding and phagocytosis of different rSpTrf::beads. The box plots show the average and interquartile range of each rSpTrf::bead treatment associated with phagocytes. Statistical analysis employed Tukey ANOVA and significance was set to $p < 0.05$. The letters above the boxplots indicate significant differences or similarities among groups. **(A, B)** The polygonal phagocytes show elevated levels of binding and phagocytosis per cell for a subset of the rSpTrf proteins compared to the other phagocyte types. They also show differential binding and phagocytosis based on the rSpTrf protein cross-linked to the beads. **(C, D)** The discoidal phagocytes bind and phagocytose fewer beads compared to the polygonal phagocytes, and do not differentiate among the rSpTrf::beads or the BSA::beads. **(E, F)** The small phagocytes do not bind or phagocytose many beads, likely due to their small size of about 5 µm, but they show differences in binding and phagocytosis depending on the rSpTrf cross-linked to the beads. Several levels of binding and phagocytosis for the different cell types and different rSpTrf::beads are shown in Table 2.

and are taken up by phagocytes, but do not enhance the phagocytosis of these beads. However, during shorter incubation times for phagocytes spun onto slides prior to the addition of beads, significantly more cells associate with rSpTrf-E1::beads compared to control beads. This discrepancy between shorter and longer incubation times may be due to more time for more phagocytes to interact with control beads, potentially masking early distinctions between the two types of beads. Compared to rSpTrf-E1, rSpTrf-E1-Ec is not glycosylated and is not stable, and its instability is exacerbated by freeze thaw cycles resulting in dimers or multimers (35) with a loss of function for binding targets (40). All of the rSpTrf proteins produced by insect cells are glycosylated and are stable over long periods, withstand multiple freeze thaw cycles, tend not to multimerize, and maintain function. In contrast to rSpTrf-E1-Ec, dimerized rSpTrf-E2-4 maintains function for binding and phagocytosis of beads by both polygonal and small phagocytes that is similar to the monomeric rSpTrf-E2-3. Although phagocytes bound fewer rSpTrf-E2-4::beads relative to those phagocytosed, this may be an outcome of more rapid uptake of the dimer by the phagocytes compared to the monomer of essentially the same protein. rSpTrf-E2-4::beads conferred greater phagocytosis compared to beads cross-linked with the other proteins. This suggests that the process of dimerization or multimerization of the natSpTrf proteins in sea urchin CF alters their function and redirects them from binding microbes or PAMPs to recognition, binding, and phagocytosis by polygonal and small phagocytes. This presents the possibility of dual functions of a subset

of natSpTrf proteins for binding to microbes and then binding to phagocytes resulting in efficient clearance of microbes.

The rSpTrf proteins produced by insect cells and the natSpTrf proteins secreted by sea urchin phagocytes are glycosylated, although it is not known whether the N-linked oligosaccharides added by these two types of cells are similar. While other types of post-translational modifications to the proteins by both types of cells are not known, they are likely present due to the relatively large molecular weights of the recombinant proteins after the removal of N-linked oligosaccharides. Antibody blocking of rSpTrf-E2-3::beads prior to cell surface binding and phagocytosis was only effective after the proteins were deglycosylated for N-linked oligosaccharides. This suggests that the locations and/or sizes of the oligosaccharides on rSpTrf-E2-3 may interfere with binding by one or more of the rabbit-anti-natSpTrf antibodies. Furthermore, deglycosylation of both rSpTrf-E1::beads and rSpTrf-E2-3::beads results in fewer phagocytes associated with beads irrespective of whether the proteins are blocked with anti-natSpTrf antibodies. This not only suggests a basis for structural stability and function of the proteins, but infers the involvement of oligosaccharides with natSpTrf protein function and immunity in sea urchins.

4.2 The rSpTrf proteins have different functions

Predictions of functional differences among the SpTrf proteins have been based on their sequence diversity (35, 36) and variations in expression levels of the genes encoding proteins of specific element patterns (30). The results presented here begin to address this hypothesis. During relatively short incubations, where only cell surface binding is assessed, a significantly greater number of phagocytes are associated with all rSpTrf::beads. This suggests that the cells have a mechanism for recognizing the rSpTrf proteins on their surfaces that may not necessarily induce phagocytosis. However, when cells are incubated with rSpTrf::beads in solution over longer periods, variations in both recognition leading to binding and phagocytosis are observed among some of the rSpTrf proteins. They show several levels of function for mediating binding and phagocytosis of beads by phagocytes. For example, rSpTrf-E2-4 and rSpTrf-E2-3, that have identical sequences but differences in dimerization, show the highest level of binding and phagocytosis. rSpTrf-A6 and rSpTrf-01 that are the largest and smallest proteins, respectively, have somewhat lower levels of activity. rSpTrf-E1, -C1, and -D1 generally show base-line, constitutive binding and phagocytosis that tend to be the same as the control BSA::beads. This infers that natSpTrf in sea urchins with different element patterns may have a variety of functions, of which some may not be involved with opsonization. rSpTrf-E1-Ec binds to *Vibrio diazotrophicus* but does not activate phagocytosis, and this may also be the case for rSpTrf-E1, -C1, and -D1. In the sea urchin immune system, native SpTrf proteins with E1, C1 and D1 element patterns may act as partners with other natSpTrf proteins to augment opsonization that leads to phagocytosis by phagocytes (38). However, different possible functions for rSpTrf proteins with these element patterns have not been explored. For example, some natSpTrf proteins may interact with microbial commensals that are present on the sea urchin surface to curtail excessive proliferation of opportunistic proliferation that may become potential pathogens (51, 71). natSpTrf proteins are also expressed by cells that are located in the gut walls (49) and the proteins may be secreted into the gut lumen and function to control the intestinal microbiome (72). Interactions between the sea urchin immune system and microbial assemblages associated with these animals has been demonstrated by the ablation of specific immune components that result in changes to the associated microbiomes (73).

The phagocytes collected from different sea urchins exhibit wide ranges in their abilities to bind and phagocytose beads cross-linked with rSpTrf proteins. These differences could be due to several possibilities. Sea urchins are collected from outbred, wild populations of animals that inhabit the west coast of North America, and *S. purpuratus* shows significant genetic differences among individual animals (74). There are also differences in the *SpTrf* gene family composition as inferred from *SpTrf* gene sequences that are not shared among individual sea urchins (31). This leads to the hypothesis that cells from different sea urchins may bind optimally to the natSpTrf proteins that are secreted by that particular animal. Consequently, cells from some animals may not be able to bind well to some of the rSpTrf proteins that originated from coelomocytes collected from different sea urchins. For example, cells collected from some sea urchins show greater association with rSpTrf-E1::beads that is similar to elevated binding by the SpTrf-E2 proteins, while cells from other sea urchins show association with rSpTrf-E1::beads that is similar to BSA::beads. This is an additional level of cellular complexity in the population and the proposed functional variations of the natSpTrf proteins in individual sea urchins expands the robustness of the echinoid immune system.

4.3 Different types of phagocytes have different functions

The large phagocytes in *S. purpuratus* are the major types of coelomocytes in the CF, making up 40% to 80% of the cells (reviewed in (64)). These cells respond to immune challenges and have been characterized as the cells that govern cellular immune responses in the purple sea urchin (75). The polygonal and discoidal phagocytes are distinct cell types with different cytoskeletal morphologies (61). They show differences in the expression of natSpTrf proteins (37), and they do not differentiate from one to the other once they appear in the CF. Coelomocytes are terminally differentiated cells that do not proliferate in the CF once they leave their sites of hematopoiesis (76), they cannot be induced to proliferate in culture (77, 78), and they do not express the transcription factors that regulate coelomocyte proliferation (39). The small and polygonal phagocytes show increased numbers and/or augmented expression of natSpTrf in response to immune challenge (37, 39, 49, 79). The results presented here suggest new and noteworthy information regarding the three types phagocytes and their capacities to interact with the different rSpTrf proteins cross-linked to beads. i) Polygonal phagocytes have been noted with more than 70 associated beads and are the major phagocytic cell in sea urchins, in agreement with a

previous report (75). They show specificity for binding and phagocytosis for a subset of rSpTrf proteins cross-linked to beads, which infers specificity for binding specific natSpTrf proteins in the CF. ii) The discoidal phagocytes are also phagocytic, but do not differentiate among the rSpTrf::beads and the BSA::beads. This may be interpreted as base-line constitutive phagocytosis of foreign particles in the absence of specific recognition of the SpTrf proteins. Discoidal cells also do not phagocytose yeast opsonized by SpC3 (65). Perhaps discoidal phagocytes have other functions in the immune system besides phagocytosis based on other opsonins bound to foreign targets. iii) The small phagocytes are phagocytic and take up rSpTrf::beads. These are the only cells to mount SpTrf proteins on the cell surface (37), which is also known for *H. erythrogramma* that has HeTrf on the surface of small phagocytes (25). The presence of natSpTrf on the cell surface and rSpTrf::beads that are phagocytosed by these cells suggests the possibility of an interaction between the rSpTrf proteins on beads and the natSpTrf proteins on the surface of small phagocytes that leads to phagocytosis. This notion is based on how readily the native Trf proteins multimerize, which is consistent for these protein in several species of sea urchins (25, 26, 37).

5 Conclusions

Of the four classes of sea urchin phagocytes, the polygonal and discoidal cells – or the large phagocytes – have generally been evaluated together and considered as a group as the major immune response cells in *S. purpuratus* (75). However, the activities of the large phagocytes presented here clearly differentiates the functions of these two types of cells. The polygonal phagocytes show specific binding and phagocytosis for a subset of rSpTrf::beads, whereas the discoidal cells show base-line, constitutive phagocytosis of all rSpTrf::beads. Although little is known about the small phagocytes (37, 50), they have been labeled as a member of the phagocyte class of coelomocytes strictly based on their morphology (39, 80). However, their capabilities to phagocytose rSpTrf::beads establishes them as phagocytes with inferences of immune functions, which is in agreement with their increase in cell numbers in response to immune challenges (37, 39, 79).

Phagocytosis and clearance of microbes from sea urchin hosts is a core function of the innate immune system in echinoids ((75, 81); reviewed in (82)). This process is universal and undertaken by most types of cells in animals, but is carried out most efficiently by professional phagocytes (83). A core aspect of phagocytosis is exemplified by the structure of the sea urchin complement system, which does not include a homologous terminal pathway for pathogen lysis, and therefore acts as an efficient opsonization system that results in phagocytosis (65, 84, 85). The importance of phagocytosis in immunity was first recognized by Elie Metchnikoff, which he demonstrated in sea star larvae (86), and is essential in other echinoderms for immune defense (66, 87). The process of phagocytosis and the proteins that are involved have been identified from transcriptomics of sea urchin coelomocytes (66). Opsonins that bind to non-self particles function as molecular linkages between a particle to be phagocytosed and the surface of the phagocyte that is an essential step in the process of phagocytosis. Our findings for the rSpTrf proteins cross-linked to inert beads infer that a subset of natSpTrf proteins in sea urchins have opsonin functions. Different versions of the rSpTrf::beads result in different levels of binding and phagocytosis by the different types of phagocytes, suggesting that different versions of the natSpTrf have a range of functions, of which one is opsonization to augment phagocytosis. There may be a variety of other activities carried out by the natSpTrf proteins that contribute to the effective host defense in echinoids. The complexity of the natSpTrf system in *S. purpuratus* is a combination of i) inferred variations in the functions of the natSpTrf proteins, ii) differences in phagocytosis functions among three types of phagocytes, and iii) genetic diversity among individual sea urchins within the population inhabiting the eastern Pacific ocean (74) that may be the basis for variations in phagocyte detection of SpTrf proteins. An integration of the complexities of SpTrf proteins, the phagocytes, and the genetic diversity among sea urchins results in an extraordinarily robust and flexible clearance system in sea urchin immunity for detecting and removing foreign particles including pathogens.

Data availability statement

The original contributions presented in the study are included in the article/Supplementary Material. Further inquiries can be directed to the corresponding author.

Ethics statement

The requirement of ethical approval was waived by George Washington University Institutional Review Board for the studies involving animals because Ethical approval was not required because research was conducted on an invertebrate animal. The studies were conducted in accordance with the local legislation and institutional requirements.

Author contributions

RC: Conceptualization, Data curation, Formal analysis, Investigation, Methodology, Software, Visualization, Writing – original draft, Writing – review & editing. CGS: Investigation, Methodology, Writing – review & editing. LG: Funding acquisition, Resources, Writing – review & editing, Methodology. LCS: Funding acquisition, Investigation, Project administration, Supervision, Writing – original draft, Writing – review & editing.

Funding

The author(s) declare financial support was received for the research, authorship, and/or publication of this article. This research was supported by an award from the US National Science Foundation (NSF IOS 1855747) to LCS and LG, and a Luther Rice Scholarship from the Columbian College of Arts and Sciences, George Washington University to CGS.

Acknowledgments

We are indebted to Cheryl Clarkson-Paredes (Imaging Center, GWU) who was essential for helping us process cells and produce the SEM images of phagocytes, and to Dr. James Stafford (University of Alberta) for essential input regarding phagocytosis. We thank Dr. Alex Jeremic (Biological Sciences, GWU) for access to and use of his confocal microscope. We are indebted to Dr. Amulya Yaparla (Biological Sciences, GWU) for instruction in protein expression with insect cells and Dr. Fang Wang (Yellow Sea Fisheries Research Institute, Chinese Academy of Fishery Sciences) who generated preliminary results demonstrating expression of rSpTrf proteins. Joseph Snitzer provided recommendations for and assisted with the statistical analyses. Archi Patel and Anthansios Naum helped in the lab.

Conflict of interest

The authors declare that the research was conducted in the absence of any commercial or financial relationships that could be construed as a potential conflict of interest.

The author(s) declared that they were an editorial board member of Frontiers, at the time of submission. This had no impact on the peer review process and the final decision.

Publisher's note

Supplementary material

The Supplementary Material for this article can be found online at: https://www.frontiersin.org/articles/10.3389/fimmu.2024.1372904/full#supplementary-material

References

1. Takeda K, Akira S. Toll-like receptors. *Curr Protoc Immunol.* (2015) 109:14.2.1–.2.0. doi: 10.1002/0471142735.im1412s109

2. Bilak H, Tauszig-Delamasure S, Imler J-L. Toll and Toll-like receptors in *Drosophila*. *Biochem Soc Trans.* (2003) 31:648–51. doi: 10.1042/bst0310648

3. Moresco EMY, LaVine D, Beutler B. Toll-like receptors. *Curr Biol.* (2011) 21: R488–R93. doi: 10.1016/j.cub.2011.05.039

4. Mathews RJ, Sprakes MB, McDermott MF. NOD-like receptors and inflammation. *Arthritis Res Ther.* (2008) 10:228. doi: 10.1186/ar2525

5. Platnich JM, Muruve DA. NOD-like receptors and inflammasomes: a review of their canonical and non-canonical signaling pathways. *Arch Biochem Biophys.* (2019) 670:4–14. doi: 10.1016/j.abb.2019.02.008

6. Chan YK, Gack MU. RIG-I-like receptor regulation in virus infection and immunity. *Curr Opin Virol.* (2015) 12:7–14. doi: 10.1016/j.coviro.2015.01.004

7. Onomoto K, Onoguchi K, Yoneyama M. Regulation of RIG-I-like receptor-mediated signaling: interaction between host and viral factors. *Cell Mol Immunol.* (2021) 18:539–55. doi: 10.1038/s41423-020-00602-7

8. Hou H GY, Chang Q, Luo T, Wu X, Zhao X. C-type lectin receptor: old friend and new player. *Med Chem.* (2017) 13:536–43. doi: 10.2174/1573406413666170510103030

9. Burdett H, Kobe B, Anderson PA. Animal NLRs continue to inform plant NLR structure and function. *Arch Biochem Biophys.* (2019) 670:58–68. doi: 10.1016/j.abb.2019.05.001

10. Saur IML, Panstruga R, Schulze-Lefert P. NOD-like receptor-mediated plant immunity: from structure to cell death. *Nat Rev Immunol.* (2021) 21:305–18. doi: 10.1038/s41577-020-00473-z

11. Tonegawa S. Somatic generation of antibody diversity. *Nature.* (1983) 302:575–81. doi: 10.1038/302575a0

12. Chien YH, Gascoigne NR, Kavaler J, Lee NE, Davis MM. Somatic recombination in a murine T-cell receptor gene. *Nature.* (1984) 309:322–6. doi: 10.1038/309322a0

13. Nagawa F, Kishishita N, Shimizu K, Hirose S, Miyoshi M, Nezu J, et al. Antigen-receptor genes of the agnathan lamprey are assembled by a process involving copy choice. *Nat Immunol.* (2007) 8:206–13. doi: 10.1038/ni1419

14. Eleftherianos I, Zhang W, Heryanto C, Mohamed A, Contreras G, Tettamanti G, et al. Diversity of insect antimicrobial peptides and proteins - a functional perspective: a review. *Int J Biol Macromol.* (2021) 30:277–87. doi: 10.1016/j.ijbiomac.2021.09.082

15. Zhang R, Xu L, Dong C. Antimicrobial peptides: an overview of their structure, function and mechanism of action. *Protein Pept Lett.* (2022) 29:641–50. doi: 10.2174/0929866529666220613102145

16. Li C, Blencke HM, Haug T, Stensvag K. Antimicrobial peptides in echinoderm host defense. *Dev Comp Immunol.* (2015) 49:190–7. doi: 10.1016/j.dci.2014.11.002

17. Sackton TM, Lazzaro BP, Clark AG. Rapid expansion of immune-related gene families in the house fly, *Musca domestica*. *Mol Biol Evol.* (2017) 34:857–72. doi: 10.1093/molbev/msw285

18. Rast JP, Smith LC, Loza-Coll M, Hibino T, Litman GW. Genomic insights into the immune system of the sea urchin. *Science.* (2006) 314:952–6. doi: 10.1126/science.1134301

19. Hibino T, Loza-Coll M, Messier C, Majeske AJ, Cohen A, Terwilliger DP, et al. The immune gene repertoire encoded in the purple sea urchin genome. *Dev Biol.* (2006) 300:349–65. doi: 10.1016/j.ydbio.2006.08.065

20. Buckley KM, Rast JP. Dynamic evolution of Toll-like recetor multigene familes in echinoderms. *Front Immunol.* (2012) 3:136. doi: 10.3389/fimmu.2012.00136

21. Buckley KM, Rast JP. Diversity of animal immune receptors and the origins of recognition commplexity in the deuterstomes. *Dev Comp Immunol.* (2015) 49:179–89. doi: 10.1016/j.dci.2014.10.013

22. Haug T, Kjuul AK, Styrvold OB, Sandsdalen E, Olsen OM, Stensvag K. Antibacterial activity in *Strongylocentrotus droebachiensis* (Echinoidea), *Cucumaria frondosa* (Holothuroidea), and *Asterias rubens* (Asteroidea). *J Invertebrate Pathol.* (2002) 81:94–102. doi: 10.1016/s0022-2011(02)00153-2

23. Arizza V, Schillaci D. Chapter 12 - Echinoderm antimicrobial peptides: the ancient arms of the deuterostome innate immune system. In: Ballarin L, Cammarata M, editors. *Lessons in immunity From Single-Cell Organisms to Mammals*. Cambridge MA, USA: Academic Press (2016). p. 159–76.

24. Smith LC, Lun CM. The *SpTransformer* gene family (formerly *Sp185/333*) in the purple sea urchin and the functional diversity of the anti-pathogen rSpTransformer-E1 protein. *Front Immunol.* (2017) 8:725. doi: 10.3389/fimmu.2017.00725

25. Roth MO, Wilkins AG, Cooke GM, Raftos DA, Nair SV. Characterization of the highly variable immune response gene family, *He185/333*, in the sea urchin, *Heliocidaris erythrogramma*. *PloS One.* (2014) 9:e62079. doi: 10.1371/journal.pone.0062079

26. Yakovenko I, Donnyo A, Ioscovich O, Rosental B, Oren M. The diverse Transformer (Trf) protein family in the sea urchin *Paracentrotus lividus* acts through a collaboration between cellular and humoral immune effector arms. *Int J Mol Sci.* (2021) 22:6639. doi: 10.3390/ijms22136639

27. Rast JP, Pancer Z, Davidson EH. New approaches towards an understanding of deuterostome immunity. *Curr Topics Microbiol Immunol.* (2000) 248:3–16. doi: 10.1007/978-3-642-59674-2_1

28. Smith LC, Chang L, Britten RJ, Davidson EH. Sea urchin genes expressed in activated coelomocytes are identified by expressed sequence tags. Complement homologues and other putative immune response genes suggest immune system homology within the deuterostomes. *J Immunol.* (1996) 156:593–602.

29. Nair SV, Del Valle H, Gross PS, Terwilliger DP, Smith LC. Macroarray analysis of coelomocyte gene expression in response to LPS in the sea urchin. Identification of

unexpected immune diversity in an invertebrate. *Physiol Genomics*. (2005) 22:33–47. doi: 10.1152/physiolgenomics.00052.2005

30. Terwilliger DP, Buckley KM, Brockton V, Ritter NJ, Smith LC. Distinctive expression patterns of *185/333* genes in the purple sea urchin, *Strongylocentrotus purpuratus*: an unexpectedly diverse family of transcripts in response to LPS, beta-1,3-glucan, and dsRNA. *BMC Mol Biol*. (2007) 8:16. doi: 10.1186/1471-2199-8-16

31. Buckley KM, Smith LC. Extraordinary diversity among members of the large gene family, *185/333*, from the purple sea urchin, *Strongylocentrotus purpuratus*. *BMC Mol Biol*. (2007) 8:68. doi: 10.1186/1471-2199-8-68

32. Smith LC. Innate immune complexity in the purple sea urchin: diversity of the *Sp185/333* system. *Front Immunol*. (2012) 3:70. doi: 10.3389/fimmu.2012.00070

33. Terwilliger DP, Buckley KM, Mehta D, Moorjani PG, Smith LC. Unexpected diversity displayed in cDNAs expressed by the immune cells of the purple sea urchin, *Strongylocentrotus purpuratus*. *Physiol Genomics*. (2006) 26:134–44. doi: 10.1152/physiolgenomics.00011.2006

34. Barela Hudgell MA, Smith LC. The complex set of internal repeats in SpTransformer protein sequences result in multiple but limited alternative alignments. *Front Immunol*. (2022) 13:1000177. doi: 10.3389/fimmu.2022.1000177

35. Lun CM, Schrankel CS, Chou H-Y, Sacchi S, Smith LC. A recombinant Sp185/333 protein from the purple sea urchin has multitasking binding activities towards certain microbes and PAMPs. *Immunobiology*. (2016) 221:889–903. doi: 10.1016/j.imbio.2016.03.006

36. Lun CM, Bishop BM, Smith LC. Multitasking immune Sp185/333 protein, rSpTransformer-E1, and its recombinant fragments undergo secondary structural transformation upon binding targets. *J Immunol*. (2017) 198:2957–66. doi: 10.4049/jimmunol.1601795

37. Brockton V, Henson JH, Raftos DA, Majeske AJ, Kim YO, Smith LC. Localization and diversity of 185/333 proteins from the purple sea urchin - unexpected protein-size range and protein expression in a new coelomocyte type. *J Cell Sci*. (2008) 121:339–48. doi: 10.1242/jcs.012096

38. Chou H-Y, Lun CM, Smith LC. The SpTransformer proteins from the purple sea urchin opsonize bacteria, augment phagocytosis, and retard bacterial growth. *PloS One*. (2018) 13:e0196890. doi: 10.1371/journal.pone.0196890

39. Golconda P, Buckley KM, Reynolds C, Romanello J, Smith LC. The axial organ and the pharynx are sites of hematopoiesis in the sea urchin. *Front Immunol*. (2019) 10:870. doi: 10.3389/fimmu.2019.00870

40. Lun CM, Samuel RL, Gillmor SD, Boyd A, Smith LC. The recombinant sea urchin immune effector protein, rSpTransformer-E1, binds to phosphatidic acid and deforms membranes. *Front Immunol*. (2017) 8:481. doi: 10.3389/fimmu.2017.00481

41. Dheilly NM, Raftos DA, Haynes PA, Smith LC, Nair SV. Shotgun proteomics of coelomocytes from the purple sea urchin, *Strongylocentrotus purpuratus*. *Dev Comp Immunol*. (2013) 40:35–50. doi: 10.1016/j.dci.2013.01.007

42. Sherman LS, Schrankel CS, Brown KJ, Smith LC. Extraordinary diversity of immune response proteins among sea urchins: nickel-isolated Sp185/333 proteins show broad variations in size and charge. *PloS One*. (2015) 10:e0138892. doi: 10.1371/journal.pone.0138892

43. Dheilly NM, Nair SV, Smith LC, Raftos DA. Highly variable immune-response proteins (185/333) from the sea urchin *Strongylocentrotus purpuratus*: proteomic analysis identifies diversity within and between individuals. *J Immunol*. (2009) 182:2203–12. doi: 10.4049/jimmunol.07012766

44. Majeske AJ, Oren M, Sacchi S, Smith LC. Single sea urchin phagocytes express messages of a single sequence from the diverse *Sp185/333* gene family in response to bacterial challenge. *J Immunol*. (2014) 193:5678–88. doi: 10.4049/jimmunol.1401681

45. Vaughn JL, Goodwin RH, Tompkins GJ, McCawley P. The establishment of two cell lines from the insect *Spodoptera frugiperda* (lepidoptera; noctuidae). *In Vitro*. (1977) 13:213–7. doi: 10.1007/BF02615077

46. Hossainey MRH, Yaparla A, Uzzaman Z, Moore T, Grayfer L. A comparison of amphibian (*Xenopus laevis*) tadpole and adult frog macrophages. *Dev Comp Immunol*. (2023) 141:104647. doi: 10.1016/j.dci.2023.104647

47. Hossainey MRH, Yaparla A, Hauser KA, Moore TE, Grayfer L. The roles of amphibian (*Xenopus laevis*) macrophages during chronic frog virus 3 infections. *Viruses*. (2021) 13:2299. doi: 10.3390/v13112299

48. Scopes RK. Measurement of protein by spectrophotometry at 205nm. *Analytical Biochem*. (1974) 59:227–82. doi: 10.1016/0003-2697(74)90034-7

49. Majeske AJ, Oleksyk TK, Smith LC. The *Sp185/333* immune response genes and proteins are expressed in cells dispersed within all major organs of the adult purple sea urchin. *Innate Immunity*. (2013) 19:569–87. doi: 10.1177/1753425912473850

50. Gross PS, Clow LA, Smith LC. SpC3, the complement homologue from the purple sea urchin, *Strongylocentrotus purpuratus*, is expressed in two subpopulations of the phagocytic coelomocytes. *Immunogenetics*. (2000) 51:1034–44. doi: 10.1007/s002510000234

51. Shaw CG, Pavloudi C, Barela Hudgell MA, Crow RS, Saw JH, Pyron RA, et al. Bald sea urchin disease shifts the surface microbiome on purple sea urchins in an aquarium. *Pathog Dis*. (2023) 81:ftad025. doi: 10.1093/femspd/ftad025

52. Smith LC, Hawley TA, Henson JH, Majeske AJ, Oren M, Rosental B. Methods for collection, handling, and analysis of sea urchin coelomocytes. In: Foltz K, Hamdoun A, editors. *Methods in Cell Biology*, vol. 150, part A. Amsterdam, The Netherlands: Elsevier (2019). doi: 10.1016/bs.mcb.2018.11.009

53. Henson JH, Svitkina TM, Burns AR, Hughes HE, MacPartland KJ, Nazarian R, et al. Two components of actin-based retrograde flow in sea urchin coelomocytes. *Mol Biol Cell*. (1999) 10:4075–90. doi: 10.1091/mbc.10.12.4075

54. Pinsino A, Alijagic A. Sea urchin *Paracentrotus lividus* immune cells in culture: formulation of the appropriate harvesting and culture media and maintenance conditions. *Biol Open*. (2019) 8:bio039289. doi: 10.1242/bio.039289

55. Clarke EC, Collar AL, Ye C, Caì Y, Anaya E, Rinaldi D, et al. Production and purification of filovirus glycoproteins in insect and mammalian cell lines. *Sci Rep*. (2017) 7:15091. doi: 10.1038/s41598-017-15416-3

56. Smith LC, Britten RJ, Davidson EH. Lipopolysaccharide activates the sea urchin immune system. *Dev Comp Immunol*. (1995) 19:217–24. doi: 10.1016/0145-305x(95)00009-i

57. Majeske AJ, Bayne CJ, Smith LC. Aggregation of sea urchin phagocytes is augmented *in vitro* by lipopolysaccharide. *PloS One*. (2013) 8:e61419. doi: 10.1371/journal.pone.0061419

58. Chiaramonte M, Inguglia L, Vazzana M, Deidun A, Arizza V. Stress and immune response to bacterial LPS in the sea urchin *Paracentrous lividus* (Lamarck, 1816). *Fish Shellfish Immunol*. (2019) 92:384–94. doi: 10.1016/j.fsi.2019.06.017

59. Romero A, Novoa B, Figueras A. Cell mediated immune response of the Mediterranean sea urchin *Paracentrotus lividus* after PAMPs stimulation. *Dev Comp Immunol*. (2016) 62:29–38. doi: 10.1016/j.dci.2016.04.018

60. Inguglia L, Chiaramonte M, Arizza V, Turiak L, Vekey K, Drahos L, et al. Changes in the proteome of sea urchin *Paracentrotus lividus* coelomocytes in response to LPS injection into the body cavity. *PloS One*. (2020) 15:e0228893. doi: 10.1371/journal.pone.0228893

61. Edds KT. Cell biology of echinoid coelomocytes. I. Diversity and characterization of cell types. *J Invertebrate Biol*. (1993) 61:173–8. doi: 10.1006/jipa.1993.1031

62. Henson JH, Nesbitt D, Wright BD, Scholey JM. Immunolocalization of kinesin in sea urchin coelomocytes. Association of kinesin with intracellular organelles. *J Cell Sci*. (1992) 103:309–20. doi: 10.1242/jcs.103.2.309

63. Smith LC, Arizza V, Barela Hudgell MA, Barone G, Bodnar AG, Buckley KM, et al. Echinodermata: the complex immune system in echinoderms. In: Cooper EL, editor. *Advances in Comparative Immunology*. New York, NY, USA: Springer Publisher (2019). p. 409–501.

64. Smith LC, Ghosh J, Buckley KM, Clow LA, Dheilly NM, Haug T, et al. Echinoderm immunity. In: Soderhall K, editor. *Invertebrate Immunity. Advances in Experimental Medicine and Biology*, vol. 708 . Landes Bioscience and Spring Science+Business Media, Austin Texas (2010). p. 260–301. doi: 10.1007/978-1-4419-8059-5_14

65. Clow LA, Raftos DA, Gross PS, Smith LC. The sea urchin complement homologue, SpC3, functions as an opsonin. *J Exp Biol*. (2004) 207:2147–55. doi: 10.1242/jeb.01001

66. Zhang W, Wang Z, Leng X, Jiang H, Liu L, Li C, et al. Transcriptome sequencing reveals phagocytosis as the main immune response in the pathogen-challenged sea urchin *Strongylocentrotus intermedius*. *Fish Shellfish Immunol*. (2019) 94:780–91. doi: 10.1016/j.fsi.2019.10.002

67. Gerdol M, Venier P, Pallavicini A. The genome of the Pacific oyster *Crassostrea gigas* brings new insights on the massive expansion of the C1q gene family in bivalvia. *Dev Comp Immunol*. (2015) 49:59–71. doi: 10.1016/j.dci.2014.11.007

68. Zhang L, Li L, Guo X, Litman GW, Dishaw LJ, Zhang G. Massive expansion and functional divergence of innate immune genes in a protostome. *Sci Rep*. (2015) 5:8693. doi: 10.1038/srep08693

69. Adema CM. Fibrinogen-related proteins (FREPs) in mollusks. *Results Problems Cell Differ*. (2015) 57:111–29. doi: 10.1007/978-3-319-20819-0_5

70. Dishaw LJ, Mueller MG, Gwatney N, Cannon JP, Haire RN, Litman RT, et al. Genomic complexity of the variable region-containing chitin-binding proteins in amphioxus. *BMC Genet*. (2008) 9:78. doi: 10.1186/1471-2156-9-78

71. Shaw CG, Pavloudi C, Crow RS, Saw JH, Smith LC. Spotting disease disrupts the microbiome of infected purple sea urchins, *Strongylocentrotus purpuratus*. *BMC Microbiol*. (2024) 24:11. doi: 10.1186/s12866-023-03161-9

72. Hakim JA, Schram JB, Galloway AWE, Morrow CD, Crowley MR, Watts SA, et al. The purple sea urchin *Strongylocentrotus purpuratus* demonstrates a compartmentalization of gut bacterial microbiota, predictive functional attributes, and taxonomic co-occurrence. *Microorganisms*. (2019) 7:35. doi: 10.3390/microorganisms7020035

73. Wessel GM, Kiyomoto M, Reitzel AM, Carrier TJ. Pigmentation biosynthesis influences the microbiome in sea urchins. *Proc R Soc B*. (2022) 289:20221088. doi: 10.1098/rspb.2022.1088

74. Britten RJ, Cetta A, Davidson EH. The single-copy DNA sequence polymorphism of the sea urchin *Strongylocentrotus purpuratus*. *Cell*. (1978) 15:1175–86. doi: 10.1016/0092-8674(78)90044-2

75. Barela Hudgell MA, Grayfer L, Smith LC. Coelomocyte populations in the sea urchin, *Strongylocentrotus purpuratus*, undergo dynamic changes in response to immune challenge. *Front Immunol*. (2022) 13:940852. doi: 10.3389/fimmu.2022.940852

76. Holland ND, Phillips JH, Giese AC. An autoradiographic investigation of coelomocyte production in the purple sea urchin (*Strongylocentrotus purpuratus*). *Biol Bull*. (1965) 128:259–70. doi: 10.2307/1539554

77. Schinke H. Bildung und Ersatz der Zellelemente der Leibeshöhlenflüssigkeit von *Psammechinus miliaris* (Echinoidea) [Formation and replacement of the corpuscles in the previsceral fluid of *Psammechinus miliaris* (Echinoidea)]. *Z fur Zellforschung und Mikroskopische Anatomie*. (1950) 35:311–31.

78. Yeager JF, Tauber OE. On the haemolymph cell counts of some marine invertebrates. *Biol Bull*. (1935) 69:66–70. doi: 10.2307/1537357

79. Oren M, Rosental B, Hawley T, Kim G-Y, Agronin J, Reynolds C, et al. Individual sea urchin coelomocytes undergo somatic immune gene diversification. *Front Immunol*. (2019) 10:1298. doi: 10.3389/fimmu.2019.01298

80. Gross PS, Al-Sharif WZ, Clow LA, Smith LC. Echinoderm immunity and the evolution of the complement system. *Dev Comp Immunol*. (1999) 23:429–42. doi: 10.1016/s0145-305x(99)00022-1

81. Wang Y, Wang Q, Chen L, Li B. The lysosome-phagosome pathway mediates immune regulatory mechanisms in *Mesocentrotus nudus* against *Vibrio coralliilyticus* infection. *Fish Shellfish Immunol*. (2023) 139:108864. doi: 10.1016/j.fsi.2023.108864

82. Smith LC, Davidson EH. The echinoderm immune system. Characters shared with vertebrate immune systems and characters arising later in deuterostome phylogeny. *Ann New York Acad Sci*. (1994) 712:213–26. doi: 10.1111/j.1749-6632.1994.tb33575.x

83. Uribe-Querol E, Rosales C. Phagocytosis: our current understanding of a universal biological process. *Front Immunol*. (2020) 11:1066. doi: 10.3389/fimmu.2020.01066

84. Bertheussen K. Receptors for complement on echinoid phagocytes. II. Purified human complement mediates echinoid phagocytosis. *Dev Comp Immunol*. (1982) 6:635–42.

85. Smith LC, Crow RS, Franchi N, Schrankel CS. The echinoid complement system inferred from genome sequence searches. *Dev Comp Immunol*. (2023) 140:104584. doi: 10.1016/j.dci.2022.104584

86. Metchnikoff E. *Lectures on the comparative pathology of inflammation: delivered at the Pasteur Institute in 1891*. Starling FA, Starling EH, editors. London: Kegan Paul, Trench, Trubner & Co. Ltd (1893).

87. Xiao K, Zhang S, Li C. The complement system and complement-like factors in sea cucumber. *Dev Comp Immunol*. (2022) 136:104511. doi: 10.1016/j.dci.2022.104511

Supplementary Material

Recombinant SpTransformer proteins are functionally diverse for binding and phagocytosis by three subtypes of sea urchin phagocytes

Ryley S. Crow, Chloe G. Shaw, Leon Grayfer, L Courtney Smith

Contents **Page**

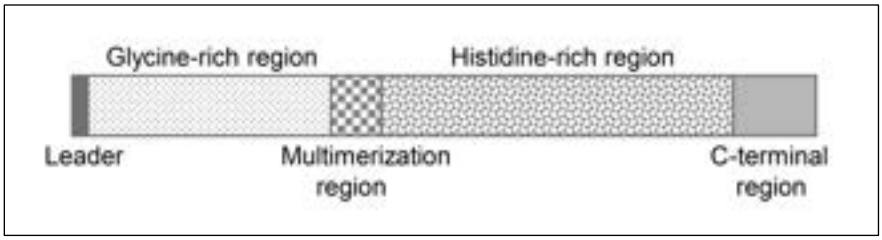

Figure S1 | General SpTrf protein structure. This figure is modified from Figure 1A in Lun et al. [1].

Figure S2 | The alignment of rSpTrf proteins shows the sequence diversity among proteins with different element patterns[1]

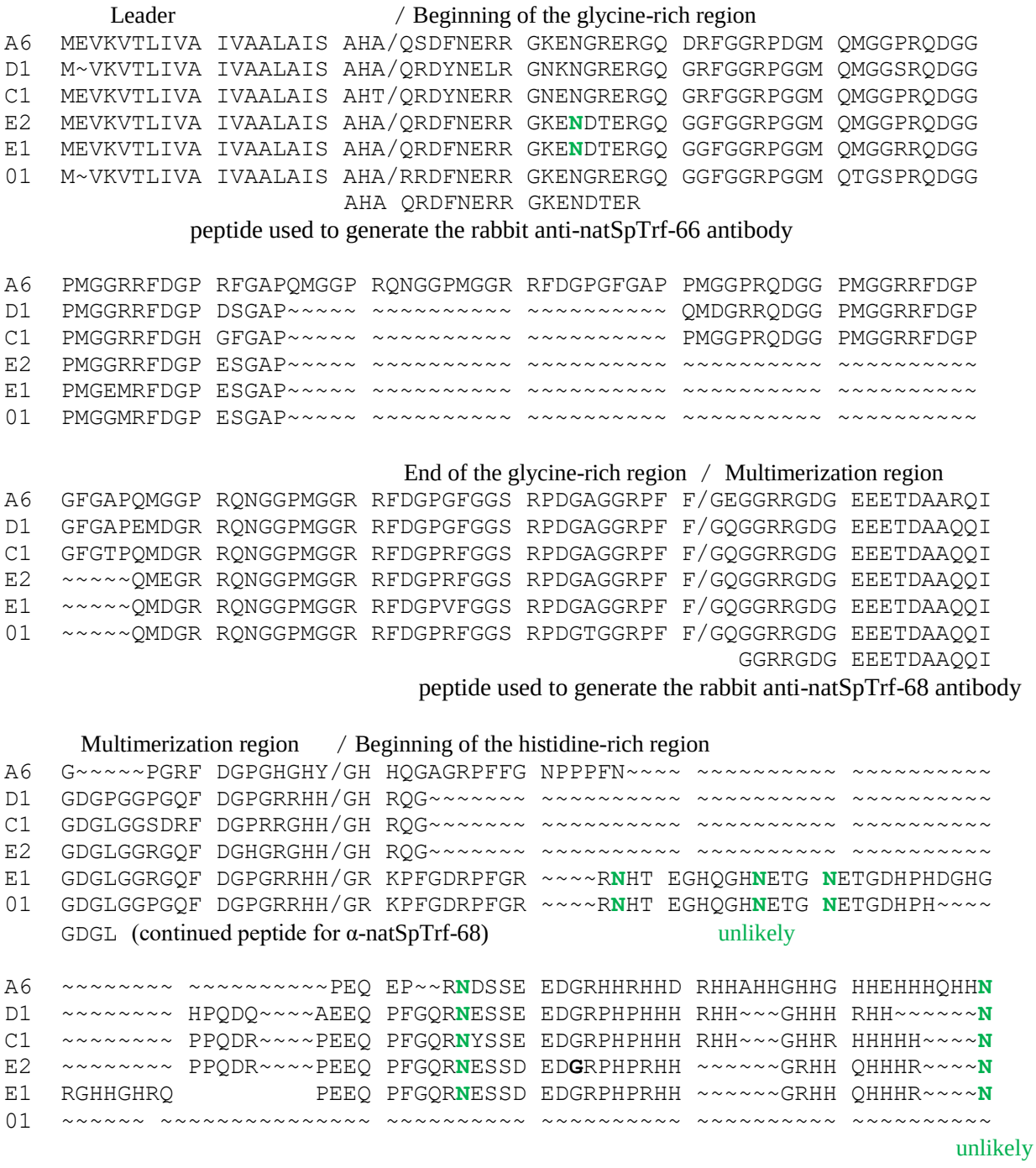

```
A6  HTEGHQ~~~~ ~~~~~~~~~~ ~~~~~DHDRP MFEMRPFRFN PLGRKPFGDH PFGRRNHTEG
D1  HTEGHQGHNE TG~~~~~~~ ~~~~DQDQDK~ LHDTRPFRYN HFGRKPFGDR PFGRRNHTEG
C1  QTEGHQGHNE TG~~~~~~~ ~~~~DQDQDKP I~DTRPFRFN HFGRKPFGGR PFGRRNHTEG
E2  HTEGHQGHNE TGDHPHRHHN KTGDGDQDRP MFEMRPFRFN PFGRKPFGDR PFGRR~~~~~
E1  HTEGHQGHNE TGDHPHRHHN KTGDGDQDRP MFEMRPFRFN PFGRKPFGDR PFGRR~~~~~
01  ~~~~~~~~~~ ~~~~~~RHHN KTRDGDQDRP MFEMRPFRFN PFGRKPFGDR PFGRR~~~~~

A6  HQGHNETGDH PHRHHSKNVD GDQDTGHHGH HGHHEHHHHQ HDHREGHQDH DRPMFEMRPF
D1  HRGHNETGDH PHRHHNKTRD GDQD~~~~~~ ~~~~~~~~~~ ~~~~~~~~~~ ~RPMFEMRPF
C1  HQGHNETGDH PHRHHNKTGD GDQD~~~~~~ ~~~~~~~~~~ ~~~~~~~~~~ ~RPMFESRPF
E2  ~~~~~~~~~~ ~~~~~~~~~~ ~~~~~~~~~~ ~~~~~~~~~~ ~~~~~~~~~~ ~~~~~~~~~~
E1  ~~~~~~~~~~ ~~~~~~~~~~ ~~~~~~~~~~ ~~~~~~~~~~ ~~~~~~~~~~ ~~~~~~~~~~
01  ~~~~~~~~~~ ~~~~~~~~~~ ~~~~~~~~~~ ~~~~~~~~~~ ~~~~~~~~~~ ~~~~~~~~~~

A6  RFNPLGRKPF GDHPFGRRNH TEGHQGHNET GDHPHRHHSK TGDGDQDRPM FETRPFWVNP
D1  RFNPFGRKPF GGRPFDRR~~ ~~~~~~~~~~ ~~~~~~~~~~ ~~~~~~~~~~ ~~~~~~~~~~
C1  RFNPFGRKPF GDRLFGRR~~ ~~~~~~~~~~ ~~~~~~~~~~ ~~~~~~~~~~ ~~~~~~~~~~
E2  ~~~~~~~~~~ ~~~~~~~~~~ ~~~~~~~~~~ ~~~~~~~~~~ ~~~~~~~~~~ ~~~~~~~~~~
E1  ~~~~~~~~~~ ~~~~~~~~~~ ~~~~~~~~~~ ~~~~~~~~~~ ~~~~~~~~~~ ~~~~~~~~~~
01  ~~~~~~~~~~ ~~~~~~~~~~ ~~~~~~~~~~ ~~~~~~~~~~ ~~~~~~~~~~ ~~~~~~~~~~

                      / C-terminal region
A6  FGRRPFGDRP FDRR/NGTEEG SPRRDGHPHP HGNRGRWGEN ESEEKEHPTT ESVTTFSPLK
D1  ~~~~~~~~~~ ~~~~/NGTEEG SPRRDGHRRP YGNRGRWGEN ESEEKEHPTT ESVTTSSPPE
C1  ~~~~~~~~~~ ~~~~/NGTEEG SPRRDGHRRP YGNRGRWGEN ESEEKEHPTT ESVTTSSPPE
E2  ~~~~~~~~~~ ~~~~/NGTEEG SPRRDGQRRP YGNRGRWGEN ESEEKEHPTM ESVTTSSPP~
E1  ~~~~~~~~~~ ~~~~/NGTEEG SARRDGQRRP YGNRGRWGEN ESEEEEHPTT ESVTTSSPP~
01  ~~~~~~~~~~ ~~~~/NGTEEG SPRRDGQRRP HGNRGRWGEN ESEEKEHPTT ESVTTSSPPE
                    GTEEG SPRRDGQRRP YGNR    unlikely
```

peptide used to generate the rabbit anti-natSpTrf-71 antibody

```
A6  VIEIAINEVD TNVVAEV
D1  VV~~AINEED INVVAEV
C1  VVEIAFNEED VNVVAEV
E2  .......... .......
E1  .......... .......
01  VVEIAIND~~ ~~~VAEV
```

[1]The alignment shows the similarities and differences among the SpTrf protein sequences chosen for expression in insect cells. Proteins are defined based on their element pattern. The alignment also shows the conserved sites for **N**-linked oligosaccharides including those that are unlikely to be linked to oligosaccharides (see Table S3). Peptides used to produce the rabbit-anti-natSpTrf antibodies are indicated on the bottom lines of the alignment [2]. The **G** at location 276 in some *SpTrf-E2* messages are edited in sea urchin cells from encoding a glycine to a stop codon resulting in truncated SpTrf-E2.1 proteins [3, 4].

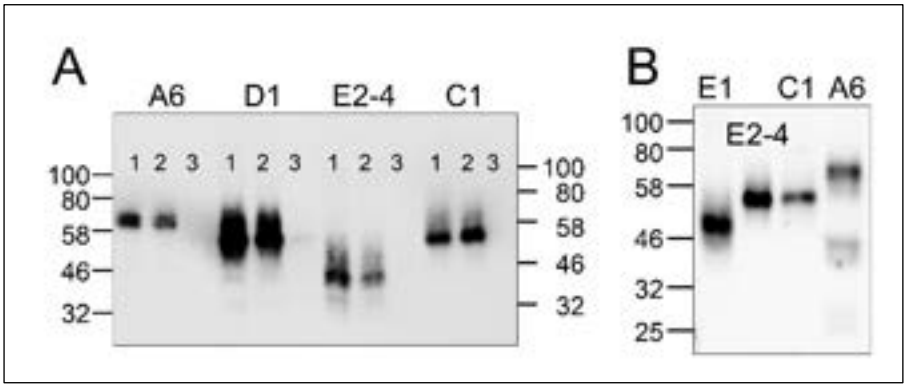

Figure S3 | rSpTrf-E2-4 increases in molecular weight over time. **(A)** A subset of rSpTrf proteins from a preliminary protein isolations prior to scaling up the culture volumes are evaluated for expression by Western blot. rSpTrf-E2-4 is ~40 kD and smaller than the other proteins on the blot. There are three lanes for each rSpTrf protein that show subsequent elutions from the Ni-NTA agarose beads (lanes 1, 2), and a sample from the media after protein isolation by nickel affinity (lane 3). **(B)** After the large scale isolation of rSpTrf proteins and storage at -80ºC for about five months, rSpTrf-E2-4 shows a molecular weight increase to about 55 kDa and is the same size as rSpTrf-C1. Both Western blots were evaluated with rabbit-anti-V5-HRP (3000X dilution: Invitrogen) followed by ECL incubation and imaging in a GelDoc Touch (BioRad) imager.

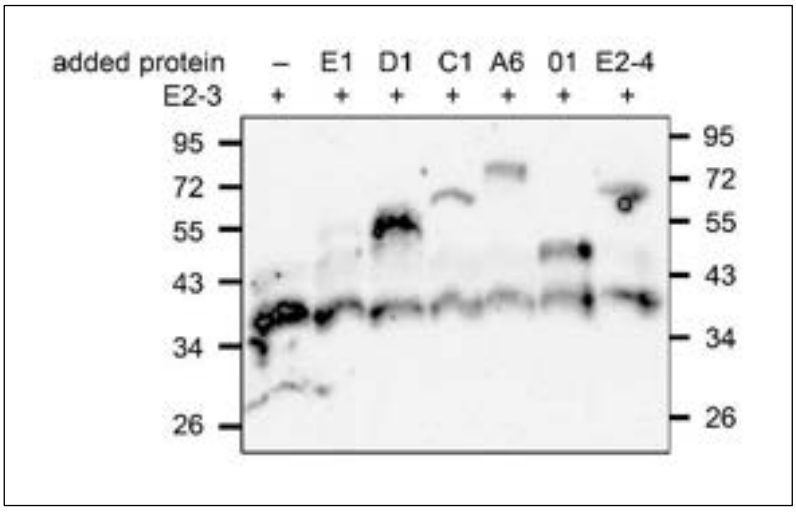

Figure S4 | The rSpTrf proteins do not multimerize with each other. rSpTrf-E2-3 was incubated with each of the other rSpTrf proteins (protein, which) at rt for 1 hr. Equal mass quantities of 1.5 µg for each protein was optimized for detection by Western blot. None of the proteins show an increase in size suggesting that multimerization does not occur. The blot was evaluated using rabbit-anti-V5-HRP (3000X dilution; Invitrogen) and imaged as in Figure S3.

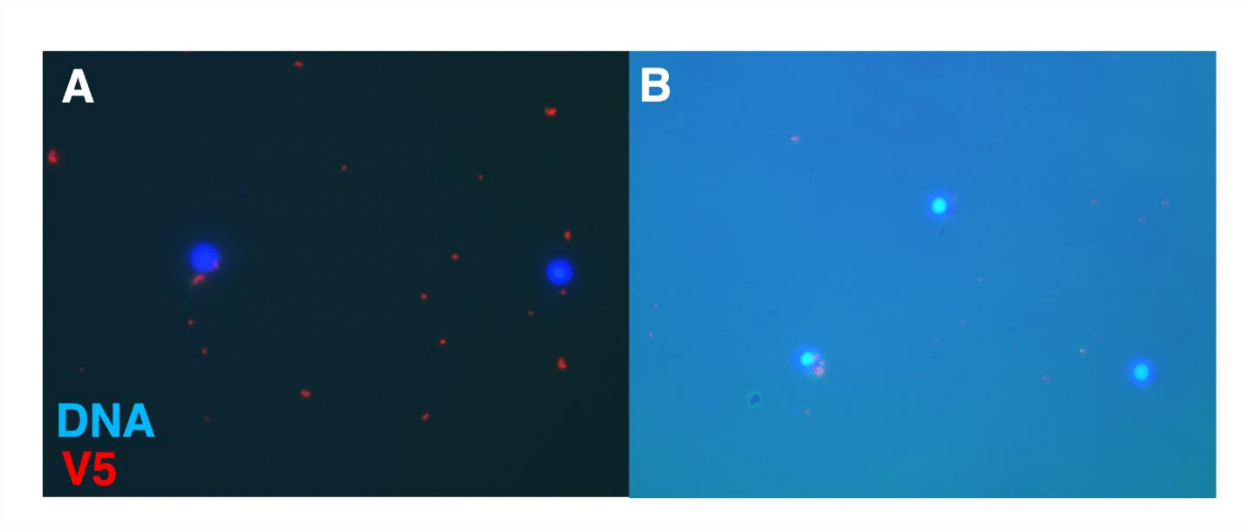

Figure S5 | Incubation of live cells with antibodies at 0ºC limits antibody binding to the surface by blocking penetration past the plasma membrane. Mouse-anti-actin antibody does not bind to the actin cytoskeleton when incubated with live coelomocytes 0°C before fixation and permeabilization. The antibody is blocked from passing through the plasma membrane. The two panels show coelomocytes from two different sea urchins **(A**, **B)**. DAPI (blue) labeling indicates the nucleus of the cells. The rSpTrf::beads (red), bound by the rabbi-anti-V5-549 (3000X dilution; Invitrogen), are on the surface of the cells. The brightfield merge for the cells from sea urchin **(A)** is unavailable. The brightfield image for the cells from animal **(B)** is shown to visualize the beads. All beads appear red indicating that are all bound to the surface of the cells. Lack of green labeling indicates that the mouse-anti-actin (1500X dilution; Invitrogen) is blocked from binding cytoskeletal actin in non-permeabilized cells and thus the goat-anti-mouse-Ig-488 (6000X; Invitrogen) antibody is negative after cells are fixed and permeabilized.

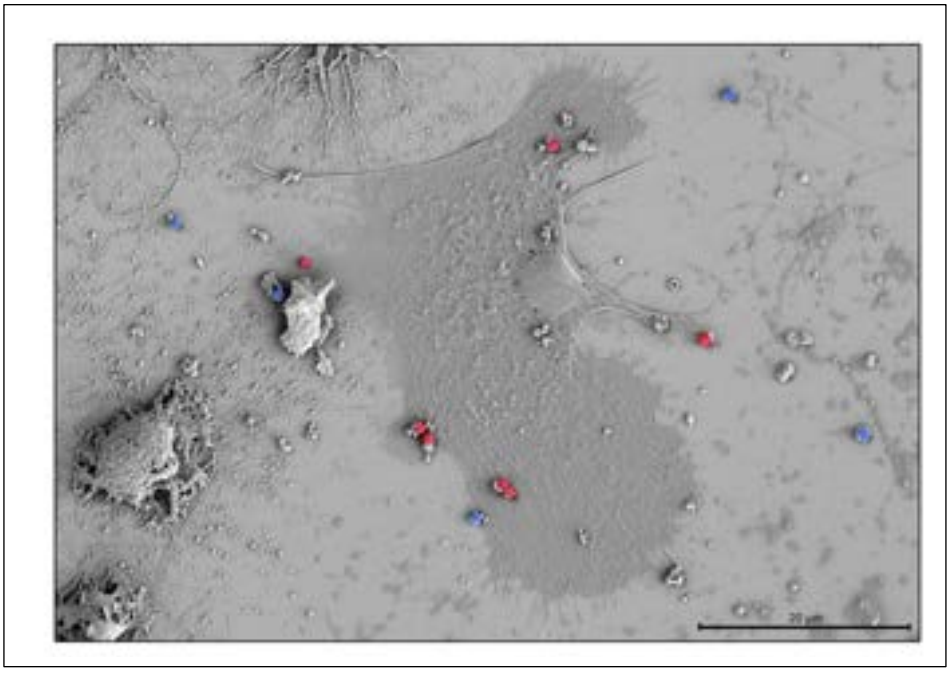

Figure S6 | Phagocytes spun onto glass slides before incubation with beads bind but do not phagocytose beads. Centrifuged cells are extremely flattened that limits cytosolic space for phagocytosis. The polygonal cell shown by scanning electron microscopy occupies 22% of the field of view area. Notably, more beads (false red color , n = 7) are observed on the cell surface than on the glass slide (false blue color, n = 5) in 78% of the area suggesting an interaction between the cell surface and the rSpTrf-E2-3::beads.

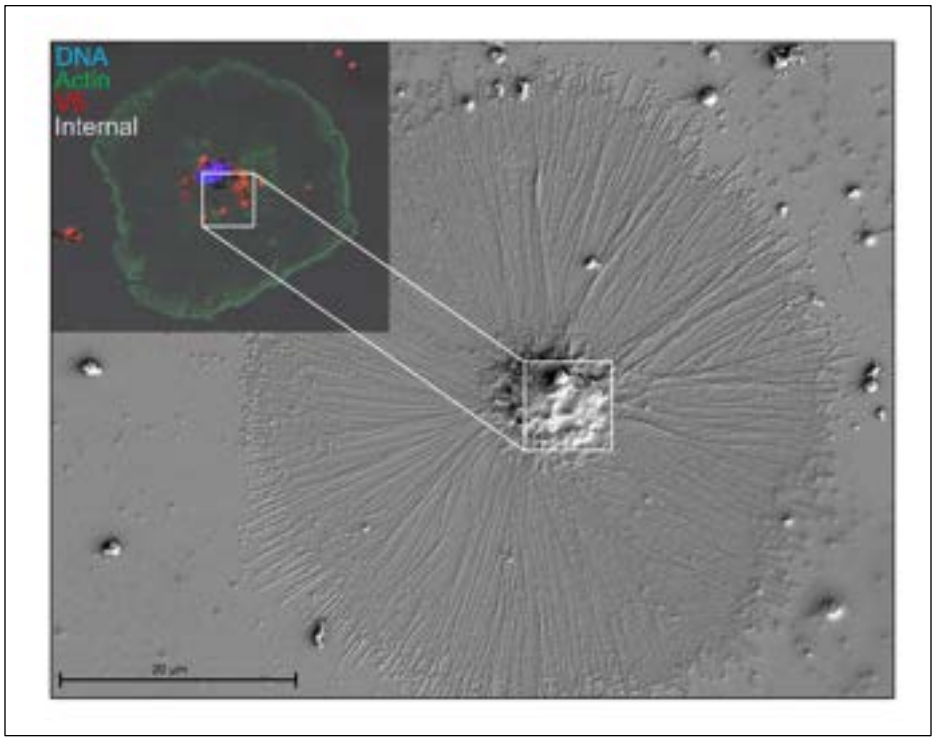

Figure S7 | Phagocytes incubated with beads in solution phagocytose beads. The scanning electron microscopy image shows a discoidal cell incubated with rSpTrf-E2-3::beads in solution. It shows a large irregular, lumpy region around the nucleus suggesting internalized beads. For comparison, the insert shows a discoidal cell by fluorescence microscopy with both surface bound and phagocytosed beads. Red beads are on the cell surface and black unlabeled beads are internal. Internal beads are positioned around the nucleus in a similar location as the irregular region at the center of the cell imaged by SEM.

Supplementary Tables

Table S1 | Primers for Gibson Assembly of the *SpTrf* cDNA sequences and the *pMIB* expression vector

Primer[1]	Sequence[2]	Length	Tm[3]	Target
01F-pMIB	GTATACATTTCTTACATCTATGCC CAAAGCGATTTCAATGAACGAC	46	65.4	*01*
01R-pMIB	GGAGAGGGTTAGGGATAG CACCTCGGCGACATCATT	36	69	
pMIBF-01	CAATGATGTCGCCGAGGTG GGTAAGCCTATCCCTAACC	38	69.9	*pMIB* for *01*
pMIBR-01	GTCGTTCATTGAAATCTCTTCG GGCATAGATGTAAGAAATGTATAC	46	65.4	
E1F-pMIB[2]	GTATACATTTCTTACATCTATGCC CAAAGAGATTTCAATGAACGACG	47	65.4	*E1, E2, E2.1*
E1R1-pMIB	GGAGAGGGTTAGGGATAG AGGTGGTGAAGATGTCGTTAC	39	68.7	*E1*
E2R-pMIB	GGGTTAGGGAGAGGCTTACC AGGTGGTGAAGATGTCGTTAC	41	70.5	*E2*
E2.1R-pMIB	GGGTTAGGGAGAGGCTTACC ATGACCATCAAACTGACCGCG	41	71.5	*E2.1*
pMIBF-E1	GTAACGACATCTTCACCACCT GGTAAGCCTATCCCTAACCC	41	69.5	*pMIB* for *E1*
pMIBR-E1	CGTCGTTCATTGAAATCTCTTTG GGCATAGATGTAAGAAATGTATAC	47	66.3	*pMIB* for *E1, E2, E2.1*
pMIBF-E2	GTAACGACATCTTCACCACCT GGTAAGCCTATCCCTAACCCT	42	71.1	*pMIB* for *E2*
AC0F-pMIB	GTATACATTTCTTACATCTATGCC CAAAGCGATTTCAATGAACGAC	46	65.4	*A6, C1, 01*
ACR2-pMIB	GGTTAGGGATAGGCTTACC CACCTCGGCGACCACAT	36	70.1	*A6, C1*
pMIBF-A	CAATGTGGTCGCCGAGG GGTAAGCCTATCCCTAAC	34	68	*pMIB* for *A6*
pMIBR-A	GTCGTTCATTGAAATCGCTTTG GGCATAGATGTAAGAAATGTATAC	46	65.4	
D1F-pMIB	GTATACATTTCTTACATCTATGCC CAAAGAGATTACAATGAACTACG	47	64.5	*D1*
D1R-pMIB	GGAGAGGGTTAGGGATAG CACCTCAGCGACCACATT	36	69	
pMIBF-D1	AATGTGGTCGCTGAGGTG GGTAATCCTATCCCTAACCC	38	68.8	*pMIB* for *D1*
pMIBR-D1	ACGTAGTTCATTGTAATCTCTTTG GGCATAGATGTAAGAAATGTATAC	48	64.6	
C1F-pMIB	GTATACATTTCTTACATCTATGCC CAAAGAGATTACAATGAACGACG	47	65.4	*C1*
C1R-pMIB	GGAGAGGGTTAGGGATAG CACCTCGGCGACCACAT	35	70.3	
pMIBF-C1	AATGTGGTCGCCGAGGTG GGTAAGCCTATCCCTAACC	37	70	*pMIB* for *C1*
pMIBR-C1	CGTCGTTCATTGTAATCTCTTTG GGCATAGATGTAAGAAATGTATAC	47	65.4	

[1]The primer name indicates the amplicon, and the target into which it will be ligated by Gibson Assembly.

[2]The upper and lower sequences correspond to the two DNA fragments that are ligated by Gibson Assembly.

[3]Tm calculations are based on www.biopho.org/minitools/melting temperature/demo

Table S2 | Primers for standard ligation of *SpTrf* inserts into the *pMIB* expression vector

Primer	Sequence	Length	Tm	Target
E2F1	CCGaagcttACAAAGAGATTTCAATGAA[1]	28	55.5	*E2, E2.1*
E2R1	GCCctcgagAGGTGGTGAAGATGTCGT[2]	27	64.3	*E2*
E2.1R1	GCGctcgagATGACCATCAAACTGACC[2]	27	62.8	*E2.1*

[1]Lower case nucleotides indicate the *Hind*III restriction site.
[2]Lower case nucleotides indicate the *Xho*I restriction site.

Table S3 | Conserved N-linked oligosaccharide positions in the rSpTrf proteins

	Number of positions	
Protein	**N[1]**	**NetNGlyc[2]**
A6	10	7
D1	8	7
C1	8	7
E2	7	5
E1	8	7
01	5	4

[1]Conserved sites for the addition of N-linked oligosaccharides are N-X(not P)-T/S.
[2]NetNGlyc is an on-line tool (https://services.healthtech.dtu.dk/services/NetNGlyc-1.0/) used to estimate the potential for glycosylation at the N positions. See the rSpTrf alignment (Figure S2) for the locations of asparagines (**N**) that could be modified with N-linked oligosaccharides.

Supplementary Text File S1

rSpTrf-E2.1 is not produced by Sf9 insect cells

The SpTrf-E2.1 version of the SpTrf-E2 protein is a truncated protein that is expressed and secreted by coelomocytes of the sea urchin, *Strongylocentrotus purpuratus* [3, 5]. The mRNA from the *SpTrf-E2* gene has a GGA encoding a glycine that is edited to, which is a stop translation codon [3]. This stop, that is present in the sequences of many cDNAs generated from mRNAs isolated from individual animals, is not present in the corresponding genes, suggesting editing of these specific messages [4]. The resulting deduced truncated protein is 14.6 kDa, and is missing most of the C terminal region that is the majority of the histidine-rich region (see above, Supplementary Figure S1). Because edited mRNAs encoding truncated SpTrf proteins decrease in prevalence upon immune challenge, it has been postulated that they may serve a surveillance function that is different from the full length proteins, of which some bind to pathogens ([6]; reviewed in [7]). To test this hypothesis, rSpTrf-E2.1 was included with the other rSpTrf proteins for production in insect cells for the purpose of characterizing protein function.

The insert from the cDNA clone 2-2439 (GenBank accession number EF065832) [3]) encodes a SpTrf protein with an E2 element pattern and was amplified by PCR to generate either the full length SpTrf-E2 protein or the truncated SpTrf-E2.1 protein using different reverse primers (Table 1.1). The amplicons were ligated into the *pMIB*/*V5*-*HisA* expression vector (ThermoFisher) using the Gibson Assembly method (New England Biolabs), transfected, grown, and isolated from *E. coli*, followed by lipofection into Sf9 insect cells with Cellfectin II reagent (Invitrogen). The rSpTrf-E2.1 and rSpTrf-E2-3 proteins were isolated from the cell culture media by nickel affinity as described in the main paper [8, 9]. When expression of rSpTrf-E2.1 by insect cell cultures was evaluated by Western blot, three different cultures failed to yield rSpTrf-E2.1 protein although rSpTrf-E2-3 was expressed and isolated successfully (Fig. 1.1). The same result was obtained when using different primary antibodies to evaluate the Western blot; either rabbit-anti-V5-HRP or a mixture of three rabbit-anti-natSpTrf antibodies.

To determine the basis for the expression failure of rSpTrf-E2.1, transfected Sf9 cells were first evaluated for whether the expression vector was incorporated into the genome. Genomic DNA (gDNA) was isolated from three cultures of insect cells; Sf9 cells transfected with *pMIB*/*V5*-*HisA* expression vector ligated with the E2.1 sequence (*pMIB-E2.1*), or transfected with *pMIB-E2-3* as the positive control, and Sf9 cells that were not transfected with an expression vector and served as the negative control. gDNA from all samples appeared to be of high quality, did not show protein contamination (Fig. 1.2A-C), were composed of large strands of DNA of greater than 10 kb (Fig. 1.2D), and supported PCR amplification of the cytoplasmic actin gene (Fig. 1.3A; Table 1.1). Amplification of the *pMIB* constructs from the gDNA template using either *pMIB* primers (Table 1.1) or *SpTrf* primers (Fig. 1.3D) indicated that both expression constructs, *pMIB-E2.1* and *pMIB-E2-3*, were incorporated into the gDNA of the Sf9 insect cells (Fig. 1.3C). Furthermore, there was no false positive amplification from the Sf9 control cells that had not been transfected with a construct (Fig. 1.3B). Amplicons produced from the gDNA were the same size as those produced from the expression vectors (Fig. 1.3C). These results indicated that the *pMIB* expression constructs were transfected into the Sf9 insect cells and that they integrated into the genome.

Given that the Sf9 cells contained the transgenes, expression of the *pMIB* constructs were evaluated to determine whether *pMIB-E2.1* was expressed compared to *pMIB-E2-3*. Total RNA

was isolated from $5X10^6$ cells from each culture using Trizol (Invitrogen). Spectrophotometry and gel analysis indicated that total RNA was isolated successfully (Fig. 1.4A-C) and that rRNA bands were observed on a gel (Fig. 1.4D). The feint smear in the gel lanes suggested the presence of mRNA. Total RNA (0.36 – 0.98 µg) was reverse transcribed with qScript cDNA synthesis kit (Quanta Bio) and evaluated by PCR for the presence of *rSpTrf-E2.1* and *rSpTrf-E2-3* messages. Results indicated that Sf9 cells transfected with either *pMIB-E2.1* or *pMIB-E2* both had RNA corresponding to the vector inserts (Fig. 1.5). This was evaluated using the SpTrf primers (Fig. 1.3D) and the primers used for Gibson Assembly (Table 1.1) and results were consistent with transgene expression. Furthermore, the amplicons from the RT-PCR reactions were the same size as those amplified directly from the expression constructs (Fig. 1.5B, C).

Given that the *pMIB* expression vectors were transfected and incorporated into the Sf9 genome, and that they drove expression of the transgenes, the last question was to determine whether the rSpTrf-E2.1 protein was produced by the Sf9 cells. Although the difference in protein isolation indicated the failure of the rSpTrf-E2.1 protein to be secreted, it did not show whether the protein was produced and secreted and then degraded in the culture media prior to isolation, whether it was produced and degraded by the cells prior to secretion, or whether it was not produced by the cells. The insect cells from the three cultures were evaluated by microscopy and the transport vesicles in the cells were quantified. To improve the visualization of vesicles among the cultures, the cells were incubated with Brefeldin A (5 µg/ml; BioLegend) for 18 hours at 27°C according to the manufacturer (see also [10]), washed in PBS to remove any secreted rSpTrf proteins, and $6X10^4$ cells were spun onto slides, fixed, and incubated with antibodies according to [2]. The primary antibodies were either i) rabbit-anti-V5-549 (3000X dilution, Rockland) or ii) rabbit-anti-natSpTrf (300X dilution, [2, 11] followed by the secondary antibody, goat-anti-rabbit Ig-555 (6000X dilution, Invitrogen). Cells were counter labeled with mouse anti-actin (1500X dilution, Invitrogen) followed by the secondary antibody goat anti-mouse Ig-488 (6000X dilution, Invitrogen), and DAPI. Background was evaluated by incubating the cells the normal rabbit serum (NRS) rather than the primary antibody. Cells were evaluated on a Axioscope fluorescence microscope (Zeiss). The percentage of cells with $V5^+$ or $SpTrf^+$ vesicles were evaluated in addition to the number of $V5^+$ or SpTrf+ vesicles per cell. Results for anti-V5 and anti-natSpTrf were the same and showed that the percentage of cells with the *pMIB-E2.1* transgene was not different from the control cells incubated with NRS or the cells that had not been transfected (Fig. 1.6A). In comparison, there were significantly more cells with $V5^+$ or $SpTrf^+$ vesicles that were transfected with the *pMIB-E2-3* expression construct. When vesicles per cell were evaluated, particularly for $\geq$ 4 vesicles per cell, the numbers of $V5^+$ or $SpTrf^+$ vesicles in cells transfected with *pMIB-E2.1* were not different from the control cells or the cells that had not been transfected (Fig. 1.6B). The control cells transfected with *pMIB-E2-3* showed significantly more $V5^+$ vesicles compared to the non-transfected control cells (Fig. 1.6C-H). This analysis suggested that the truncated rSpTrf-E2.1 protein may have been unstable and degraded by the insect cells prior to loading into transport vesicles. It is noteworthy that sea urchin coelomocytes produce and secrete this truncated version [5] indicating significant differences between insect cells and echinoid cells that may be based on post translational modifications that are addressed in the main paper.

Figures for Supplementary Text File S1

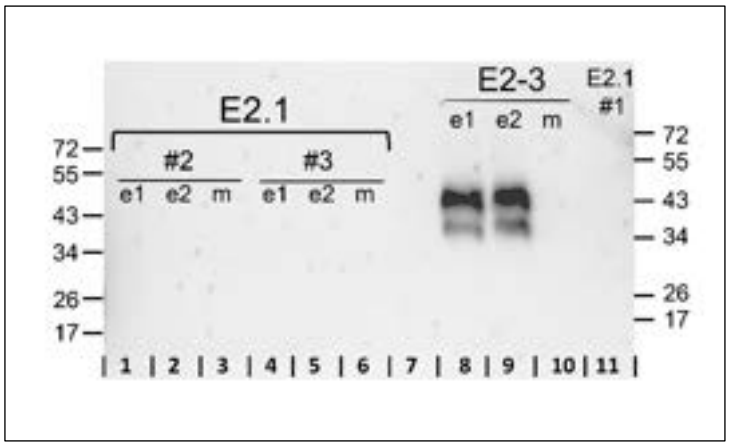

Fig. 1.1 | rSpTrf-E2.1 protein production fails repeatedly for Sf9 cell cultures. Samples from three cultures of insect cells transfected with the *pMIB-E2.1* expression construct and one culture transfected with *pMIB-E2-3* are evaluated for protein production. Results from the Western blot shows that rSpTrf-E2.1 is not isolated from culture #1 (lane 11) or from cultures #2 and #3 (lanes 1-6). Lanes 1-2 and 4-5 show the first and second elutions (e1, e2) from the Ni-NTA (Invitrogen) affinity column, and lanes 3 and 6 show the media (m) after Ni-NTA affinity protein isolation. For comparison, one insect cell culture produces rSpTrf-E2-3 (lanes 8-10). Lanes 8 and 9 are loaded with samples from the first and second elutions (e1 and e2) of rSpTrf-E2-3 from the nickel affinity column. Lane 10 shows the media (m) that after isolation by Ni-NTA affinity, in which no rSpTrf-E2-3 remains. Proteins are separated on a 15% SDS-PAGE and transferred to PVDF filters (Immobillon-P^{sq}, Millipore) by electroblotting (Trans Blot Turbo transfer system, BioRad), and the filter is evaluated with rabbit-anti-V5-HRP (3000X dilution; Invitrogen), incubated in SuperSignal^{TM} West Pico PLUS Chemiluminescent Substrate according to the manufacturer (ThermoScientific), and imaged in a ChemiDoc Touch imaging system (BioRad). When duplicate blots are evaluated with rabbit-anti-natSpTrf antibodies [11, 12], similar negative results for rSpTrf-E2.1 are obtained (not shown). Protein standard (Broad Range, ThermoFisher) sizes are indicated.

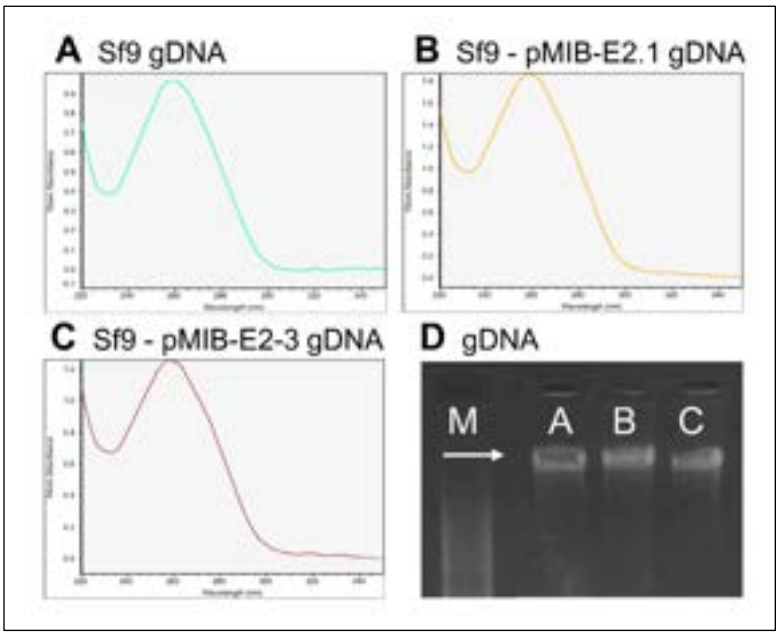

Fig. 1.2 | Genomic DNA is isolated from Sf9 cell cultures. Genomic DNA was isolated from $5X10^6$ insect cells with the GeneJET gDNA purification kit (Fermentas). **(A – C)** OD^{260} readouts by spectrophotometry (NanoDrop 2000c, ThermoScientific) are shown for the genomic DNA isolated from the three cell cultures. Scans indicate no contamination with proteins. **D**. Isolation from the Sf9 cultures yields large, non-degraded genomic DNA of >10 kb (arrow). Lane letters correspond to the scans in panels **A**, **B**, and **C**. Each lane is loaded with about 100 ng of gDNA and separated on a 0.75% agarose gel in Tris-acetate-EDTA buffer (TAE; 40 mM Tris; 20 mM acetic acid, 1 mM EDTA) with ethidium bromide. The DNA standard is loaded in lane M. The gel was imaged with the Kodak Molecular Imaging System (Kodak Gel Logic 1500) under ultraviolet light.

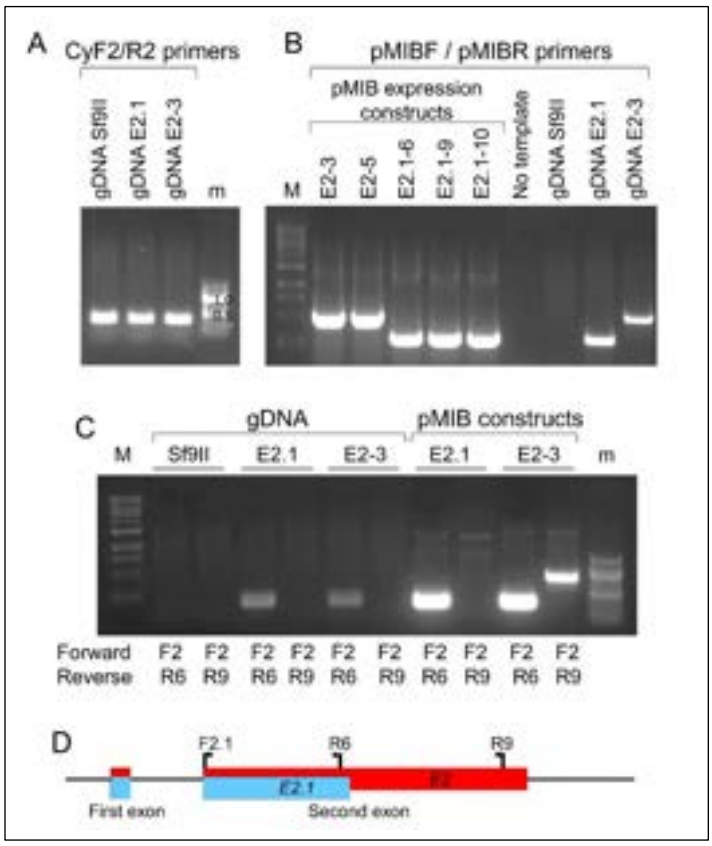

Fig. 1.3 | PCR amplification of gDNA from Sf9 insect cells indicates that the pMIB expression vectors are incorporated into the genome. **(A)** To ensure that the Sf9 insect cell gDNA can support PCR, primers (Table S1) for cytoplasmic actin (Cy) are used to amplify the actin gene. Amplicons of the expected size are obtained. **(B)** Primers for *pMIB* show amplicons for *pMIB-E2.1*. Several *pMIB* expression constructs are evaluated for insert sizes using primers specific for *pMIB* sequences that flank the inserts. These *pMIB* constructs have the same insert sequence, but are transfected into Sf9 cells at different times followed by different isolations of the rSpTrf-E2 proteins. Both *pMIB-E2-3* and *-E2-5* constructs amplified inserts of the expected size. Three *pMIB-E2.1* constructs (*-6, -9, -10*) amplified smaller inserts of the expected size. (*pMIB-E2.1-10* was chosen for all subsequent analyses.) When the *pMIB* primers are used with the gDNA template isolated from cells transfected with *pMIB-E2-3* or with *pMIB-E2.1*, the amplicon sizes match those of the constructs. No amplicons are observed when the template is gDNA from Sf9 cells that had not been transfected with a *pMIB* expression construct or when the template is omitted. **(C)** Primers specific for *SpTrf* sequences amplify *SpTrf-E2.1* and *SpTrf-E2-3* sequences from Sf9 gDNA. To verify the results using the *pMIB* primers, *pMIB* constructs and gDNA are used as templates for primers specific for the *SpTrf* sequences. Both *F2.1*/*R6* and *F2.1*/*F9* primer pairs (Table S1) that are specific for *SpTrf* sequences, amplify the insert of the *pMIB-E2-3* construct. Because the insert for *E2.1* is truncated, only the *F2.1*/*R6* primer pair amplifies the insert. When these SpTrf primer pairs are used with gDNA from Sf9 cells transfected with *pMIB-E2.1* as the template, the amplicon generated by the *F2.1*/*R6* primers is the expected size of the *E2.1* construct insert. gDNA from Sf9 cells transfected with *pMIB-E2-3* amplified with *F2.1*/*R6* and *F2.1*/*R9* primer pairs results in amplicons of the expected sizes. gDNA from non-transfected Sf9 cells do not support amplification with *SpTrf* primers. Sizes of the DNA standards are shown in **(A)**. The gels are 0.8% agarose in TAE running buffer with ethidium bromide. The gels were imaged under ultraviolet light with the Kodak Molecular Imaging system (Kodak Gel Logic 1500). **(D)** *SpTrf* primer locations are shown. A standard structure of an *SpTrf* gene is shown. *SpTrf-E2* is indicated in red, while the truncated version, *SpTrf-E2.1*, is indicated in blue. The overlapping regions have identical sequence.

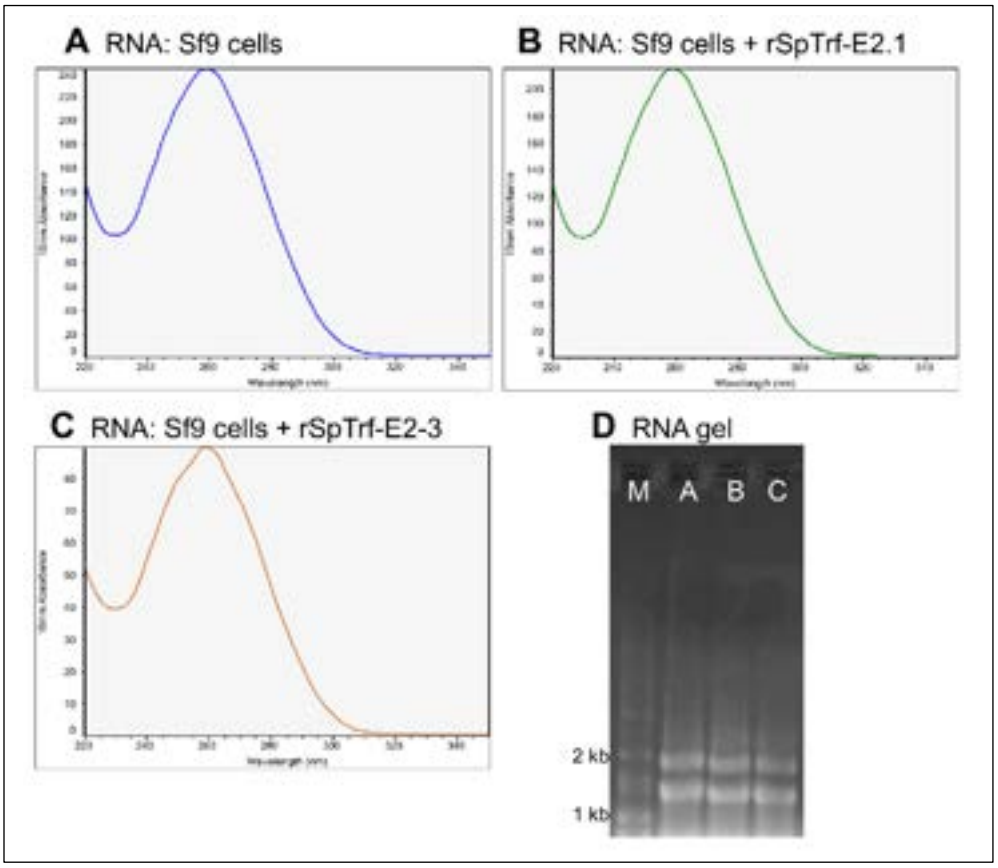

Fig. 1.4 | The *pMIB* expression constructs drive transcription and message accumulation in the Sf9 cells. Total RNA isolation for each cell culture was carried out according to the method for Trizol (Invitrogen). **(A-C)** Evaluation of the RNA concentration by spectrophotometry for OD^{260} (NanoDrop 2000c, ThermoFisher) indicates the presence of nucleic acids in all samples. **(D)** RNA from each sample was loaded onto a 0.8% agarose gel with TAE and ethidium bromide. Lane A, RNA (0.97 µg) from Sf9 cells; lane B , RNA (0.86 µg) from Sf9 cells transfected with *pMIB-E2.1* expression construct; lane C, RNA (0.36 µg) from Sf9 cells transfected with *pMIB-E2-3* expression construct. The bands at about 1.4 kb and 2.0 kb are tRNA and the smear is likely mRNA. Imaging under UV light was done in Kodak Molecular Imaging system (Kodak Gel Logic 1500). Standard DNA marker sizes are indicated (lane M).

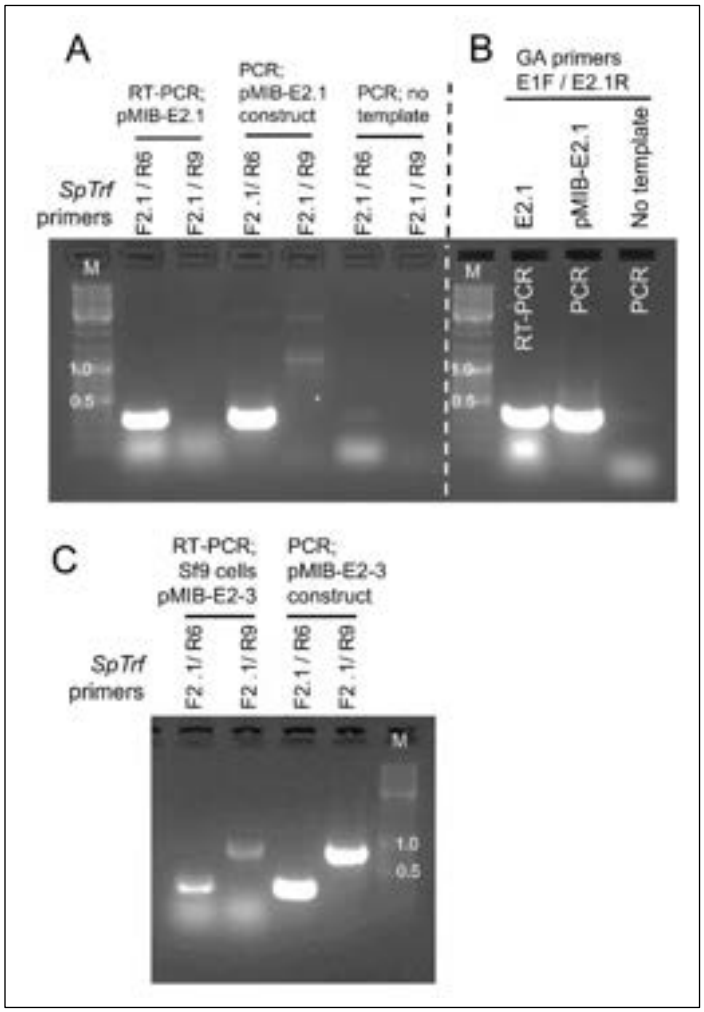

Fig. 1.5 | The *pMIB-E2.1* construct is expressed in Sf9 cells. **(A)** Reverse transcription of total RNA isolated from Sf9 cells transfected with *pMIB-E2.1* followed by PCR (RT-PCR) with the *F2.1*/*R6* primers (Table 1.1) shows that the cells contain mRNA from the expression vector. The amplicon from the Sf9 cells is the same size as the amplicon generated by PCR of the *pMIB-E2.1* construct. Amplification with the *F2.1*/*R9* primers fails because the *E2.1* sequence does not include the *R9* annealing site (see Fig. 1.3D). The gel image in **(A)** has been edited to remove duplicate lanes. **(B)** RT-PCR of total RNA isolated from Sf9 cells transfected with *pMIB-E2.1* with the primers used to amplify the cDNA insert for Gibson Assembly (GA) Cloning (*E1F*/*E2.1*(*pMIB*)*R*; Table 1.1), shows that the cells contain mRNA from the expression vector. The amplicon generated by PCR from the expression construct with the same GA primers is the same size. (Note that the *E1F* primer amplifies both *E1* and *E2* sequences.) **(C)** RT-PCR of total RNA isolated from Sf9 cells transfected with *pMIB-E2-3* with both *F2.1*/*R6* and *F2.1*/*R9* primers result in two sizes of amplicons. PCR with *pMIB-E2-3* results in the same two sizes of amplicons. This shows that the *F2.1*/*F9* primers function as expected. Relevant sizes in the GeneRuler DNA standards (ThermoFisher) are indicated. See Fig. 1.3D for the locations of the SpTrf primers.

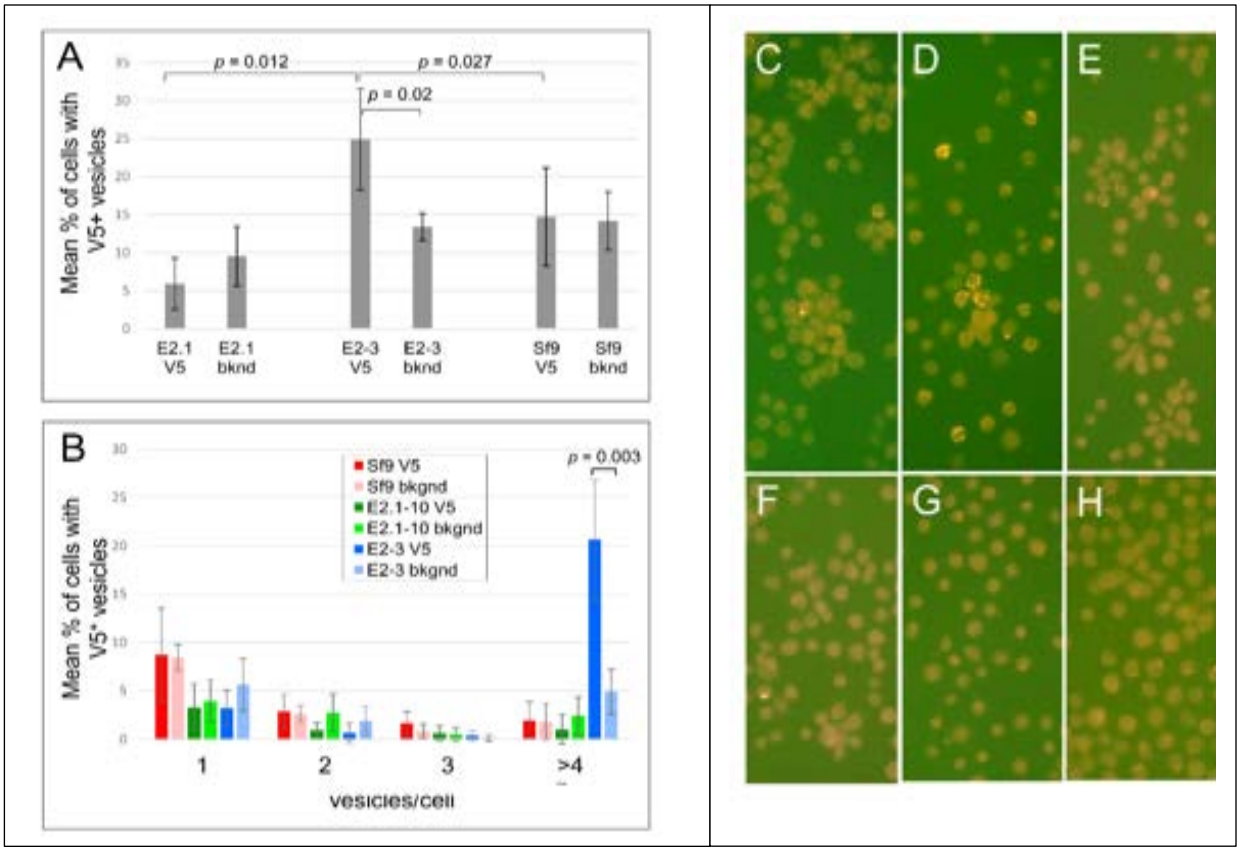

Fig. 1.6 | rSpTrf-E2.1 is not produced by Sf9 cells compared to rSpTrf-E2-3. Three cultures of Sf9 cells, un-transfected cells, cells transfected with the *pMIB-E2.1* construct, and cells transfected with the *pMIB-E2-3* construct, were incubated with Brefeldin A (5 µg/ml, BioLegend) for 18 hours at 27ºC to block secretion. This treatment accumulated transport vesicles in the cells to augment differences among the three cultures. Cells were fixed and incubated with rabbit-anti-V5 or with normal rabbit serum followed by goat-anti-rabbit-Ig-549 (bkgnd, background). **(A)** The mean percentage of cells with one or more $V5^+$ vesicles is shown for each culture. The percentage of cells with rSpTrf-E2.1 in transport vesicles is not different from background, whereas the percentage of cells with rSpTrf-E2-3 in transport vesicles is significantly more than cells expressing rSpTrf-E2.1, or background levels in Sf9 cells. **(B)** Sf9 cells transfected with *pMIB-E2.1* do not produce rSpTrf-E2.1 proteins. The number of $V5^+$ vesicles per cell for Sf9 cells transfected with *pMIB-E2.1* is not different from cells that were not transfected with an expression vector. In contrast, cells transfected with *pMIB-E2-3* have significantly more $V5^+$ vesicles compared to background. Significance for all comparisons was established by the two tailed *t*-test ($p < 0.05$). **(C-H)** Results in **(B)** were obtained from fluorescence microscopy images of cells with $V5^+$ vesicles **(C-E)** compared to background **(F-H)**. **(C**, **F)** Cells transfected with rSpTrf-E2.1, **(D**, **G)** cells transfected with rSpTrf-E2-3, **(E**, **H)** un-transfected Sf9 cells.

Table for Supplementary Text File 1

Table 1.1 | Primers used in PCR

Primer	Sequence	Tm, °C
E1(pMIB)F[1]	gtatacatttcttacatctatgccCAAAGAGATTTCAATGAACGACG	65.4
E2.1(pMIB)R[2]	gggttagggagaggcttaccATGACCATCAAACTGACCGCG	71.5
E2(pMIB)R[3]	gggttagggagaggcttaccAGGTGGTGAAGATGTCGTTAC	70.5
pMIBF[4]	GCGCGCCTATAAATACAGC	56.0
pMIBR[4]	GACAATACAAACTAAGATTTAGTCAG	54.4
CyF2[5]	GTGACGACGATGTTGCCGC	64.5
CyR2[5]	TTGGGGTTGAGGGGAGCC	64.5
SpTrf-F2.1[6]	AGMGATTWCAATGAACKRCGAGGA	62.0
SpTrf-R6[6]	CGAGCATCAGTTTCTTTCKTCTC	61.7
SpTrf-R9[6]	CTTHARGTGGTGGAARATGTCG	59.3

[1]This forward primer anneals to the 5' end of 2-2439 cDNA [3], and was designed to generate a 5' ligation region for cloning into the *pMIB* vector by Gibson Assembly (New England BioLabs). It is used to amplify both *E1* and *E2* sequences. Lower case nucleotides indicate the sequence match to *pMIB*. Upper case nucleotides indicate the sequence match to the *SpTrf* insert sequence.

[2]This reverse primer anneals to the middle of 2-2439 cDNA to amplify the truncated version of *E2*, termed *E2.1*. The primer was designed to produce a 3' ligation site for cloning into the *pMIB* vector by Gibson Assembly. Lower case nucleotides indicate the sequence match to *pMIB*. Upper case nucleotides indicate the sequence match to the SpTrf insert sequence.

[3]This primer anneals to the 3' end of the coding region of 2-2436 cDNA amplify the full length *E2* insert. It was designed for cloning into the *pMIB* vector by Gibson Assembly. Lower case nucleotides indicate the sequence match to *pMIB*. Upper case nucleotides indicate the sequence match to the SpTrf insert sequence.

[4]This primer pair surrounds the insert and was used to amplify all *SpTrf* inserts.

[5]*Cy*, cytoplasmic actin.

[6]See Fig. 1.3D for the locations of the *SpTrf* primers.

Supplementary Text File S2

The initial approach to evaluate phagocytosis of rSpTrf::beads by sea urchin phagocytes used magnetic attraction of cells associated with beads

The functions of the natSpTrf proteins were originally speculated to act as opsonins that bind to foreign cells and PAMPs to augment phagocytosis. The first functional characterization of a recombinant SpTrf protein had an E1 element pattern, rSpTrf-E1, and it bound to *Vibrio diazotrophicus* [12], but did not augment its phagocytosis by sea urchin coelomocytes [11]. It was proposed that this might be a characteristic of natSpTrf proteins with an E1 element pattern, and that other natSpTrf isoforms would function differently, resulting in an effective immune protection system. To test this hypothesis, cells that phagocytosed magnetic beads that were cross-linked to different molecules or left non cross-linked, were evaluated after attraction to a magnet, as has been reported for isolating phagosomes from phagocytes [13]. CF was collected from sea urchins in calcium- and magnesium-free sea water with EDTA and HEPES buffer (CMFSW-EH; 460 mM NaCl, 10.7 mM KCl, 7.04 mM Na_2SO_4, 2.38 mM $NaHCO_3$, 70 mM EDTA, 20 mM HEPES pH 7.4; [14]) and the cells were pelleted at 500 x *g* for 5 min and resuspended in coelomocyte culture medium (CCM; 0.5 M NaCl, 5 mM $MgCl_2$, 1 mM EGTA, 20 mM HEPES, pH 7.4; [2, 15]). rSpTrf-E2-3, rSpTrf-E2-4, and BSA were cross-linked to 1 µm magnetic COOH-beads (Bangs Laboratories) by the 2-step EDAC cross-linking method (Polysciences). BSA cross-linked to COOH-beads (BSA::beads) served as the negative control. Streptavidin (SA)-beads (Bangs Laboratory) were incubated with LPS-biotin (LPS::beads) from *E. coli* (0111:B4 strain; Invivogen) according to the manufacturer (Bangs Laboratory) and served as the positive control. Control SA-beads were processed similarly, but LPS-biotin was omitted. Beads were incubated in solution with coelomocytes (50:1) in 500 µl CCM at 14ºC for 20 min. Cells containing beads were collected by magnetic attraction for 15 min on ice. The supernatant was moved to a new tube, which contained cells that were not attracted to the magnet, and cells in the capture fraction were washed once with CCM, and resuspended into 50 µl CCM. The average number of beads per cell was evaluated by microscopy and significant differences in the average number of beads per cell among the different cross-linked beads were identified with a Tukey ANOVA test. Results showed that the average number of beads per cell was significantly higher for LPS::beads, and beads cross-linked to rSpTrf-E2-3, and -E2-4, compared to COOH-beads (Fig. 2.1). However there was no significant difference between the LPS::beads, rSpTrf-E2-3::beads, and the rSpTrf-E2-4::beads compared to the BSA::beads. This suggested a problem with the assay because the average number of LPS::beads (positive control) per cell was not different from the BSA::beads (negative control).

To determine whether this unexpected result was an outcome of the relatively short incubation time for cells to interact with beads (20 min), the experiment was repeated using several time points (0, 10, 20, 60, 90 min), and followed the same magnetic capture method described above. This was undertaken to determine whether longer incubation periods would reveal differences for cells with phagocytosed beads. Cell were counted for each fraction using microscopy, and the average percentage of cells collected by the magnet was calculated based on the total number of cells in both the magnet capture fraction and the supernatant. Results showed that for incubations with each bead treatment, the average percentage of cells attracted to the magnet remained unchanged and did not increase at longer time periods (Fig. 2.2). At the 90 min time point, the percentage of cells incubated with BSA::beads was lower than at 0 min. Furthermore, there were cells present in the magnet capture fraction at 0 min for all bead

treatments, which was unexpected and unlikely that the cells had time to phagocytose beads. When the cell types were evaluated by microscopy, there were phagocytes with beads in the magnet capture fraction, but there were also phagocytes without beads. Furthermore, this fraction contained all types of coelomocytes without beads including red and colorless spherule cells and vibratile cells that are not known to be phagocytic (reviewed in [16, 17]). These results suggested that all types of coelomocytes bound to the walls of the plastic tubes and that the assay did not evaluate phagocytosis. The results also suggested that cells that had phagocytosed beads and were attracted to the magnet were subsequently mixed with cells that had bound to the tube wall during incubations and included cells without beads. Consequently, the outcome identified a large background effect that confounded attempts to characterize phagocytosis of beads cross-linked to different molecules.

To confirm whether any cells captured by the magnet had phagocytosed beads, cells were pre-treated with cytochalasin D (cytoD, 32 µM; SigmaAldrich) for 30 minutes. This treatment inhibited actin polymerization and consequently blocked phagocytosis. Following the above protocol cytoD treated and un-treated cells were incubated with COOH-beads for 20 min and the cells in both the magnet and supernatant fractions were counted using microscopy. Cells were found in the magnet capture even when treated with cytoD (Fig. 2.3). Furthermore, cytoD treated cells did not show significant differences in the average percentage of cells in the magnet capture fraction compared to cells that were not treated with cytoD. These results indicated that the magnet based capture and analysis of cells that had bound and/or phagocytosed magnetic beads was not feasible for sea urchin coelomocytes because all cell types bound to the plastic tube walls. Consequently, an alternative method was developed to incubate the cells with beads followed by evaluation by microscopy. Because the phagocytes bound tightly to glass, whereas other coelomocyte types did not and were removed by washes, the evaluation of phagocyte detection and phagocytosis of cross-linked beads was employed (see the main paper).

Figures for Supplementary Text File 2

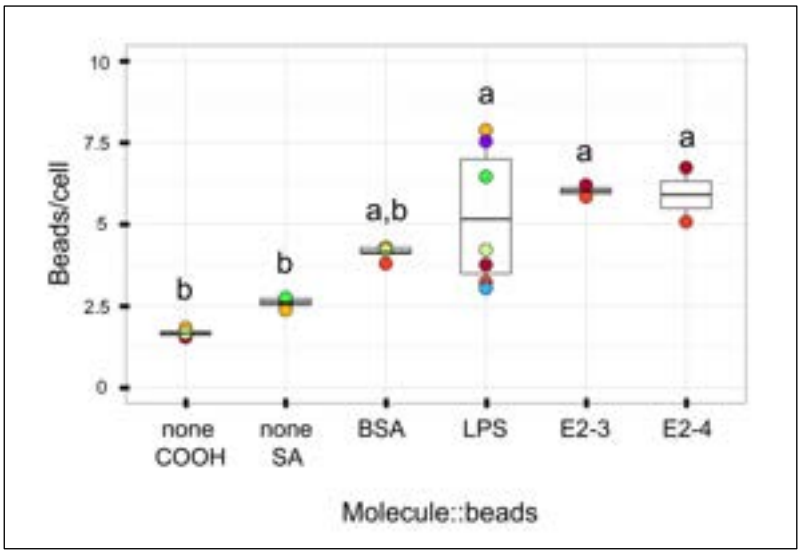

Fig. 2.1 | Phagocytes do not differentiate among beads cross-linked with rSpTrf proteins, LPS, or BSA. Cells were incubated with beads for 20 min and the number of beads per cell was evaluated for cells captured by the magnet. COOH (beads not cross-linked to a molecule), SA (beads not cross-linked to a molecule). Beads cross-linked with BSA, LPS, or rSpTrf proteins are indicated. The box plots show the average and interquartile range of each bead treatment associated with phagocytes and results for cells from different sea urchins are identified by colored dots. Significant differences were determine by a Tukey ANOVA test (see Methods section 2.9 in the main paper). The letters above the boxplots indicate significant differences and similarities.

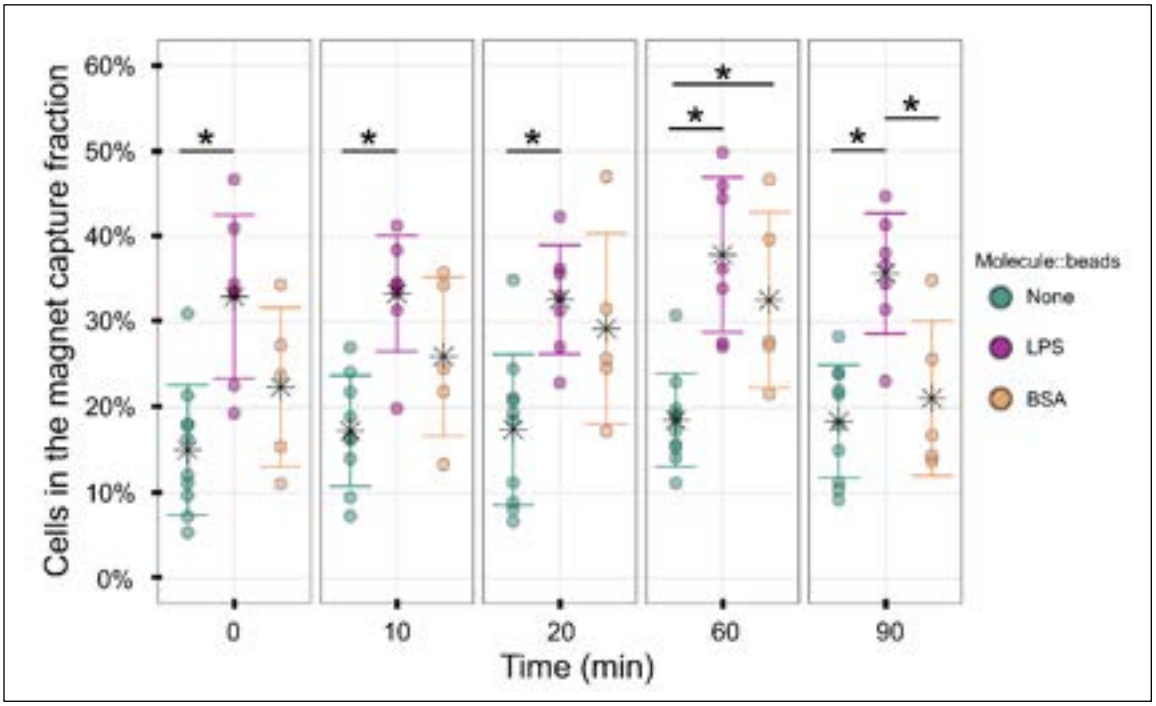

Fig. 2.2 | Cells in the magnet capture fraction are present at all time points. The average number of cells that were associated with beads cross-linked to LPS or BSA or non-cross-linked COOH-beads was evaluated by microscopy. Black stars indicate the average number of cells in the magnet capture fraction, and error bars show the standard deviation for each bead type tested. Significant differences were determined using a Tukey ANOVA test for each time point. Results are approximately the same for the three bead types across all time points, including results at 0 min. *, $p < 0.05$.

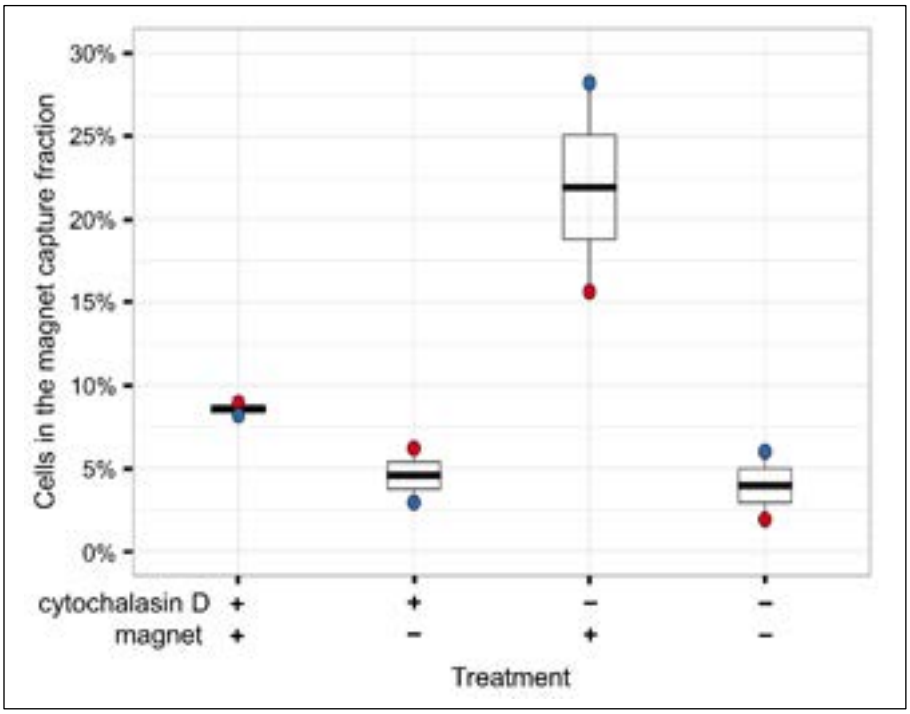

Fig. 2.3 | Coelomocytes are present in the magnet capture fraction irrespective of treatment with cytochalasin D. Cells incubated with cytochalasin D to block phagocytosis followed by incubation with COOH-beads are present in both the magnet capture fraction and the supernatant containing cells that are not attracted by the magnet. Omitting cytochalasin D did not show significant changes to the percentage of cells in the magnet capture fraction. The box plots show the average and interquartile range of each treatment associated with phagocytes, and none of the treatments are significantly different based on a Tukey ANOVA test (see Methods section 2.9 in the main paper).

References

1. Lun CM, Samuel RL, Gillmor SD, Boyd A, Smith LC. The recombinant sea urchin immune effector protein, rSpTransformer-E1, binds to phosphatidic acid and deforms membranes. Frontiers in Immunology. 2017;8:481. doi: 10.3389/fimmu.2017.00481
2. Brockton V, Henson JH, Raftos DA, Majeske AJ, Kim YO, Smith LC. Localization and diversity of 185/333 proteins from the purple sea urchin - unexpected protein-size range and protein expression in a new coelomocyte type. Journal of Cell Science. 2008;121(3):339-48. doi: 10.1242/jcs.012096
3. Terwilliger DP, Buckley KM, Brockton V, Ritter NJ, Smith LC. Distinctive expression patterns of *185/333* genes in the purple sea urchin, *Strongylocentrotus purpuratus*: an unexpectedly diverse family of transcripts in response to LPS, beta-1,3-glucan, and dsRNA. BMC Molecular Biology. 2007;8:16. doi: 10.1186/1471-2199-8-16
4. Buckley KM, Terwilliger DP, Smith LC. Sequence variations in *185/333* messages from the purple sea urchin suggest posttranscriptional modifications to increase immune diversity. Journal of Immunology. 2008;181:8585-94. doi: 10.4049/jimmunol.181.12.8585barella
5. Dheilly NM, Nair SV, Smith LC, Raftos DA. Highly variable immune-response proteins (185/333) from the sea urchin *Strongylocentrotus purpuratus*: proteomic analysis identifies diversity within and between individuals. Journal of Immunology. 2009;182:2203-12. doi: 10.4049/jimmunol.07012766
6. Sherman LS, Schrankel CS, Brown KJ, Smith LC. Extraordinary diversity of immune response proteins among sea urchins: nickel-isolated Sp185/333 proteins show broad variations in size and charge. PLoS ONE. 2015;10(19):e0138892. doi: 10.1371/journal.pone.0138892
7. Smith LC, Lun CM. The *SpTransformer* gene family (formerly *Sp185/333*) in the purple sea urchin and the functional diversity of the anti-pathogen rSpTransformer-E1 protein. Frontiers in Immunology. 2017;8:725. doi: 10.3389/fimmu.2017.00725
8. Hossainey MRH, Yaparla A, Uzzaman Z, Moore T, Grayfer L. A comparison of amphibian (*Xenopus laevis*) tadpole and adult frog macrophages. Developmenal and Comparative Immunology. 2023;141:104647. doi: 10.1016/j.dci.2023.104647
9. Hossainey MRH, Yaparla A, Hauser KA, Moore TE, Grayfer L. The roles of amphibian (*Xenopus laevis*) macrophages during chronic frog virus 3 infections. Viruses. 2021;13(11):2299. doi: 10.3390/v13112299
10. Lovelace P, Maecker HT. Multiparameter intracellular cytokine staining. In: Hawley T, Hawley, R., editor. Flow Cytometry Protocols Methods in Molecular Biology. Methods in Molecular Biology. 3rd ed. Totowa, NJ, USA: Humana Press; 2011. p. 165-78. doi: 10.1007/978-1-61737-950-5_8
11. Chou H-Y, Lun CM, Smith LC. The SpTransformer proteins from the purple sea urchin opsonize bacteria, augment phagocytosis, and retard bacterial growth. PLoS One. 2018;13(5):e0196890. doi: 10.1371/journal.pone.0196890
12. Lun CM, Schrankel CS, Chou H-Y, Sacchi S, Smith LC. A recombinant Sp185/333 protein from the purple sea urchin has multitasking binding activities towards certain microbes and PAMPs. Immunobiology. 2016;221:889-903. doi: 10.1016/j.imbio.2016.03.006
13. Pryor PR, P. RA. Isolating phagosomes from tissue culture cells. Cold Spring Harbor Protocols. 2014;12:1320-3. doi: 10.1101/pdb.prot074468

14. Smith LC, Hawley TA, Henson JH, Majeske AJ, Oren M, Rosental B. Methods for collection, handling, and analysis of sea urchin coelomocytes. In: Foltz K, Hamdoun A, editors. Methods in Cell Biology. 150, part A: Elsevier; 2019. doi: 10.1016/bs.mcb.2018.11.009
15. Henson JH, Svitkina TM, Burns AR, Hughes HE, MacPartland KJ, Nazarian R, et al. Two components of actin-based retrograde flow in sea urchin coelomocytes. Molecular Biology of the Cell. 1999;10(12):4075-90. doi: 10.1091/mbc.10.12.4075
16. Smith LC, Ghosh J, Buckley KM, Clow LA, Dheilly NM, Haug T, et al. Echinoderm immunity. In: Soderhall K, editor. Invertebrate Immunity. Advances in Experimental Medicine and Biology. 708. Austin Texas: Landes Bioscience and Spring Science+Business Media; 2010. p. 260-301. doi: 10.1007/978-1-4419-8059-5_14
17. Smith LC, Arizza V, Barela Hudgell MA, Barone G, Bodnar AG, Buckley KM, et al. Echinodermata: The complex immune system in echinoderms. In: Cooper E, editor. Advances in Comparative Immunology: Springer Publisher; 2018. p. 409-501.